Rapport quadriennal de la Section VII Sciences physiques des Océans

pour le congrès IUGG 2011

Contenu

Rapport quadriennal IUGG de la Section 7 "Sciences Physiques de l'Ocean"

Observations of the ACC across the Kerguelen Plateau: TRACK project

PI: Young-Hyang Park (yhpark@mnhn.fr)
LOCEAN/DMPA, Muséum National d'Histoire Naturelle, Paris, France

Rational and objectives

The Kerguelen Plateau is the largest near-meridional submarine topographic obstacle, diverting the Antarctic Circumpolar Current (ACC) over a great distance between the subtropical and subpolar regions. It acts as a natural barrier for closing the eastern boundary of the Weddell Gyre to the west and developing the western boundary of the Australian-Antarctic Gyre to the east of the plateau, thus providing an important meridional pathway for the equatorward evacuation of transformed subpolar water masses. Despite its indisputable role in the ACC dynamics and the Southern Ocean meridional circulation, our knowledge on the physics and dynamics of the ACC across the Kerguelen Plateau has been seriously hampered until recently due to lacking of high-quality oceanographic observations. The TRACK (Transport across the Kerguelen Plateau) cruises carried out as part of a French contribution to the International Polar Year activities, were designed to measure directly the top-to-bottom physical properties, currents and transport over the Kerguelen Plateau, especially across the Fawn Trough and the Deep Western Boundary Current (DWBC) on the eastern flank of the southern plateau.

TRACK cruises and preliminary results

In February-March 2009 closely-spaced, full-depth hydrographic and direct current measurements in the Fawn Trough area were made during the TRACK cruise (Chief Scientist: Y.-H. Park) on R/V Marion Dufresne II. This cruise occupied in particular a near-meridional section across the Fawn Trough and repeated the western boundary segment of the WOCE I8S section at 58°S (Fig. 1). Three lines of current meter mooring with a total of 12 current meters were maintained for about 1 year across the Southern ACC Front (SACCF), which were recovered in January 2010 during the TRACK recovery cruise (Chief Scientist: F. Vivier). The preliminary results from the 2009 TRACK cruise (Park et al., 2009) are summarised below, while the velocity time series data from recovered current meters are under analysis as part of a thesis work.

Vertical profiles of cross-track lowered acoustic Doppler current profiler (LADCP) velocities and corresponding transport across the western (SACCF) and southern (DWBC) sections are shown in Figure 2. In the western section most of the eastward flow is tightly concentrated in the Fawn Trough, with the strongest flow of 0.6 m s-1 at the surface decreasing to 0.3 m s-1 at 1000 m, below which the velocity is nearly constant reaching >0.2 m s-1 at 2000 m, indicating that both the baroclinic and barotropic components of current are equally important. A secondary eastward flow branch with a depth-averaged velocity on the order of 0.2 m s-1 is observed on the near-shore slope just south of the Heard/McDonald Islands. The net transport across this 750 km-long western section amounts to 50 Sv (1 Sv = 106 m3 s-1) northeastward, 43 Sv of which are concentrated at the SACCF and 6 Sv immediately south of the Heard/McDonald Islands. In the southern section the northwestward flowing DWBC is highly barotropic and mostly confined within a narrow (~75 km) continental slope. It is also characterized by a bottom-intensified flow, with the highest velocity >0.3 m s-1 being found at the bottom at station 48. The total transport of the DWBC amounts to 43 Sv, which is largely compensated by a poleward recirculation transport of 34 Sv in the offshore area.

The TRACK cruise has permitted us to evaluate for the first time reliable transport values of different ACC branches crossing the Kerguelen Plateau (Fig. 3). Including ~2 Sv inferred at the Polar Front (PF) branch south of the Kerguelen Islands, the net ACC transport to the south of the islands amounts to 58 Sv: 43 Sv at the SACCF passing through the Fawn Trough; 6 Sv south of the Heard/McDonald Islands; 7 Sv at the Southern Boundary (SB) of ACC through the northern Princess Elizabeth Trough. The latter 7 Sv was obtained by considering only those stations in the southern section where the bottom water has a temperature >0.1°C, while the major component (36 Sv) of the DWBC with a bottom temperature <0.1°C should be fed by the northward turning of the Antarctic Slope Current along the western limb of the cyclonic subpolar gyre. According to previous work, the ACC main branch associated with the Subantarctic Front (SAF) should carry 89-94 Sv north of the Kerguelen Islands and ~6 Sv at the PF just east of the islands. Combining these with the TRACK transports sums up to 147-152 Sv as the total ACC transport in the Kerguelen area, which are not significantly different from the 147±10 Sv at 140°E south of Australia and the Drake Passage transport of 137±8 Sv augmented by 10-15 Sv of the Indonesian Throughflow.

Reference

PARK Y.-H., VIVIER F., ROQUET F. & KESTENARE E., 2009. - Direct observations of the ACC transport across the Kerguelen Plateau, Geophys. Res. Lett., 36: L18603, doi:10.1029/2009GL039617.

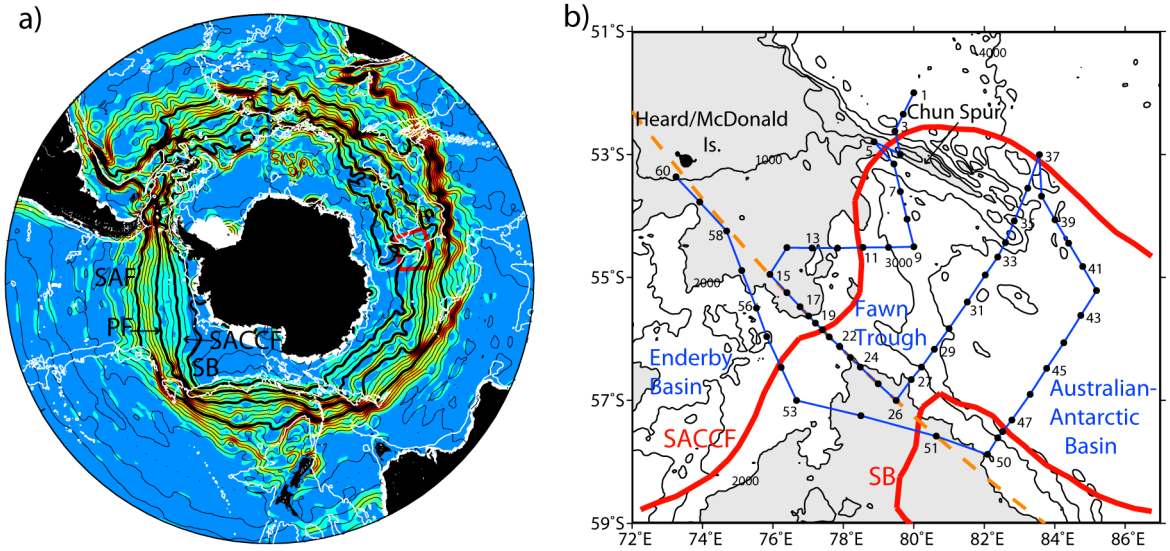

Fig.1_Park. (a) Surface streamlines from the altimetry-derived mean dynamic height, with bold streamlines standing for four circumpolar fronts and a red box for the TRACK cruise area. (b) the 2009 TACK cruise map showing the grid of 60 CTD stations, with two southernmost circumpolar fronts being superimposed. A dotted line is the Jason altimeter ground track #94. Adapted from Park et al. (2009).

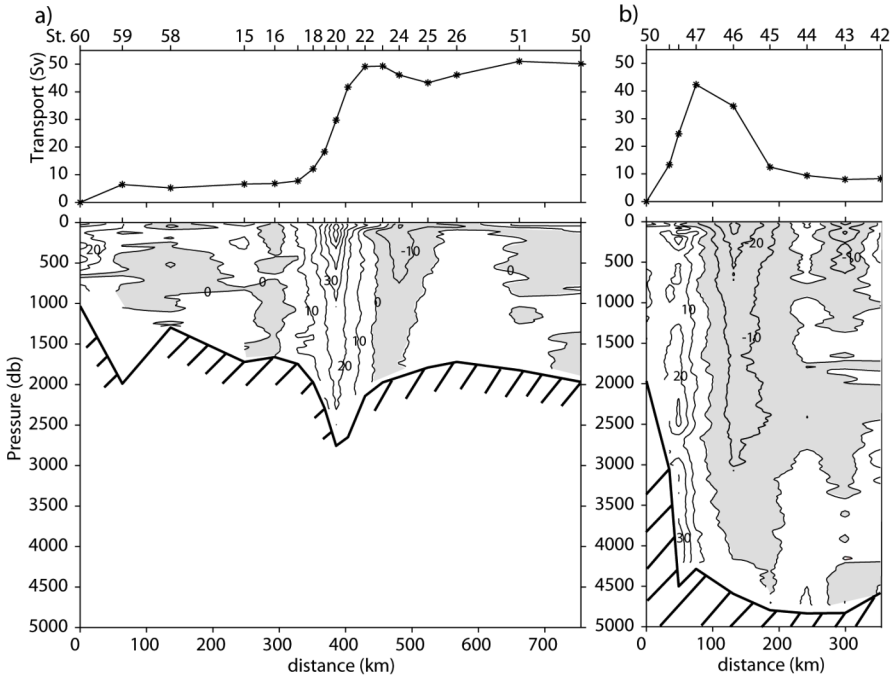

Fig. 2_Park. Vertical profiles of cross-track LADCP velocities and cumulative top-to-bottom transport in the (a) western (Fawn Trough) and (b) southern (DWBC) sections. Adapted from Park et al. (2009).

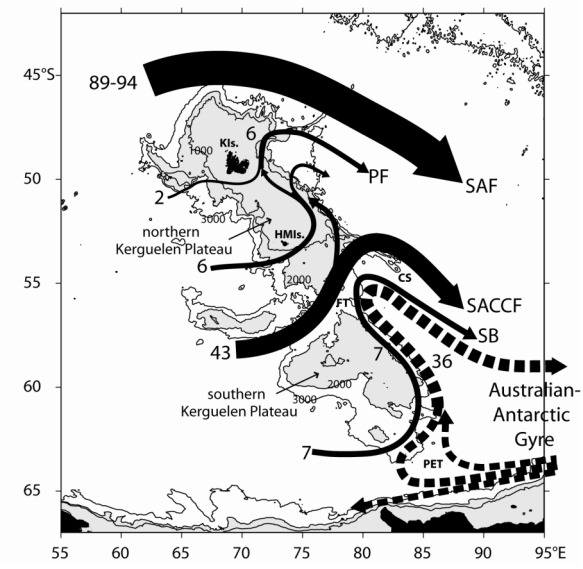

Fig. 3_Park. Schematic of major pathways and transports (in Sv) of the ACC system (bold continuous lines) and DWBC of the Australian-Antarctic Gyre (bold discontinuous lines). Adapted from Park et al. (2009).

Figure captions

Fig.1_Park. (a) Surface streamlines from the altimetry-derived mean dynamic height, with bold streamlines standing for four circumpolar fronts and a red box for the TRACK cruise area. (b) the 2009 TACK cruise map showing the grid of 60 CTD stations, with two southernmost circumpolar fronts being superimposed. A dotted line is the Jason altimeter ground track #94. Adapted from Park et al. (2009).

Fig. 2_Park. Vertical profiles of cross-track LADCP velocities and cumulative top-to-bottom transport in the (a) western (Fawn Trough) and (b) southern (DWBC) sections. Adapted from Park et al. (2009).

Fig. 3_Park. Schematic of major pathways and transports (in Sv) of the ACC system (bold continuous lines) and DWBC of the Australian-Antarctic Gyre (bold discontinuous lines). Adapted from Park et al. (2009).

The DRAKE project - Experimental aims and design

Young-Hyang Park, Christine Provost

The DRAKE project is a recently concluded experiment consisting of in situ measurements made over a period of about 3 years (February 2006 to April 2009), which are tightly coupled to satellite altimetry (TOPEX/POSEIDON and Jason). A major goal of DRAKE is to attempt to combine in situ current meter observations with simultaneous satellite data from Jason to gain a better understanding of the relationship between sea surface height (SSH) and volume transport. The measurement array consisted of 10 subsurface current meter moorings deployed below Jason track 104, with individual moorings located at altimeter crossover points (Fig. 1). High resolution hydrography and LADCP measurements were made on the cruises that serviced the moorings [Provost et al., 2011]. All cruises were performed from R.V. Polarstern. A total of 5 full-depth hydrographic sections were performed.

DRAKE early results

Early results from analyses of satellite data and the Drake hydrographic data are summarized below, while the time series from the moorings are under analysis as parts of two Ph.D. thesis.

The altimetric time-series documented the long-term trends in sea surface height, the recurrence of major frontal meanders and statistical links between them (Barré et al., 2011). Trends are not homogeneous in Drake Passage, rather they change sign, suggesting a regional effect caused by the complicated bathymetry and geometry (Fig. 2). Topography favors the recurrence of some meanders and eddies in specific spots in Drake Passage. For example a dipole occurring with a close to annual periodicity is observed at the entrance to DP over the Phoenix Antarctic Ridge (PAR) and corresponds to adjacent meanders of the SAF and PF (Barré et al., 2011) (Fig. 3). An anticyclonic meander of the PF was found to be recurrent over the Ona sea floor depression (OSD) to the northwest of the Ona Basin (54°W, 58°S) and constitutes an important element of the cyclonic recirculation in the Ona Basin (Barré et al., 2008).

Barre et al. [2011] used isolines of absolute dynamic topography from satellite altimetry data to map out locations of fronts and eddies, providing a temporal and spatial context for the 2006 DRAKE mooring deployment cruise. Multiple branches of ACC fronts were observed to merge into single jets in the narrowest part of the passage, with two branches of the SAF merging at about 61°W and three branches of the PF merging over the Shackleton Fracture Zone (SFZ) (Fig. 4 a and b). The SACCF branches could also be traced using altimetry. The agreement between the location of the frontal branches and eddies detected by altimetry and the patterns observed in sea surface temperature and ocean color is remarkable in spite of the differences in spatial and temporal resolution (Fig. 4 c, d, e). The crest of the SFZ constitutes a barrier in the south of DP, causing the two SACCF branches to separate by about 400 km, creating sheltered conditions in partial isolation from the ACC, while promoting an active recirculation region in the Ona Basin (Fig. 4 c, d, e). This recirculation, marked by cyclonic eddies carrying cold fresh and oxygenated water from south of the Southern Boundary of the ACC (Fig. 4 c, d, e), causes effective ventilation of the whole Circumpolar Deep Water (CDW) density range (Provost et al., 2011).

The 2006 cruise comprised a hydrographic section under Jason-1 track 104 repeated within 3 weeks, providing a unique opportunity to document full depth in situ variability at about a 10-day interval. Between the two occupations, the contributions of frontal meanders and eddies to the total volume transport changed notably, although the net transport changed by only 10% and agreed within confidence limits with prior WOCE and ISOS estimates [Renault et al., 2011]. Due to high quality of the data and a fine horizontal resolution, transport was estimated (143 Sv) with the best accuracy ever achieved of 7-10 Sv.

Considerable differences in properties between the 10-day-apart sections are observed throughout the whole water column with values as high as 0.2°C in temperature, 0.01 in salinity, 0.03 kg.m-3 in neutral density and 10 μmol.kg-1 in dissolved-oxygen concentration found below a depth of 3000 m [Provost et al., 2011; Sudre et al., 2011]. Only part of the differences is attributable to frontal or eddy displacements along the section. The other part results from the spatial heterogeneity of water properties upstream the section and the funnelling of the flow due to the topographic constraints of the Shackleton Fracture Zone (SFZ). The considerable short-term differences in water properties in rather large-scale structures that cannot be accounted for by frontal motions along the section, call for caution when interpreting differences in hydrographical properties obtained by oceanographic cruises that are years apart in terms of climatic signals.

References:

Barré N., C. Provost, N. Sennéchael, J. Hak Lee, 2008: Circulation in the Ona Basin, southern Drake Passage. J. Geophys. Res., 113, doi:10.1029/2007JC004549

Barré N., C. Provost, A. Renault, N. Sennéchael, 2011: Mesoscale activity in Drake Passage during the January-February 2006 cruise: a satellite perspective. Deep Sea Res., Part II, Topical Studies in Oceanography (in press)

Provost C., A. Renault, N. Barré, N. Sennéchael, V. Garçon, J. Sudre and O. Huhn, 2011: Two repeat crossings of Drake Passage in austral summer 2006: short term vatiations and evidence for considerable ventilation of intermediate and deep waters. Deep Sea Res., Part II, Topical Studies in Oceanography.

Renault A., C. Provost, N. Sennéchael, N. Barré and A. Kartavtseff, 2011: Two LADCP surveys in the Drake Passage in 2006: transport estimates. Deep Sea Res., Part II, Topical Studies in Oceanography, (in press).

Sudre J., V. Garçon, C. Provost, N. Sennéchael, O. Huhn, and M. Lacombe, 2011: Short-term variations of deep water masses in Drake Passage revealed by a multiparametric analysis of the ANT-XXIII/3 bottle data Deep Sea Res., Part II, Topical Studies in Oceanography, (in press).

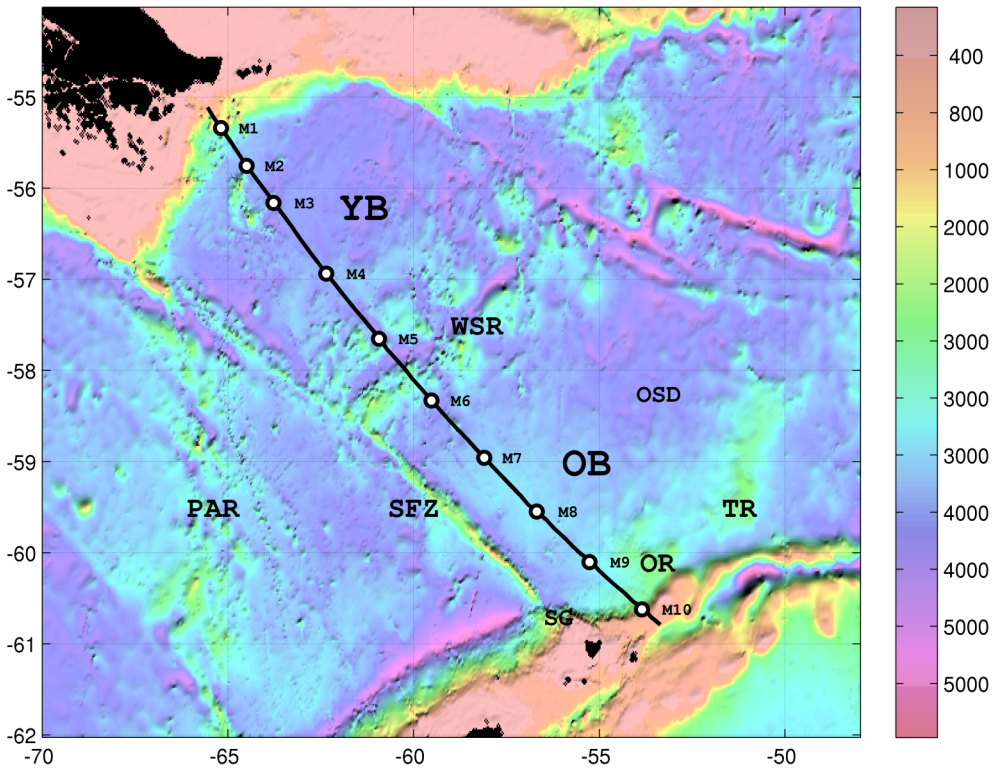

Figure 1: Location of the 10 Drake current meter moorings M1 through M10)along Jason ground track #104. Background is bathymetry in meters. Major bathymetric features are labeled: YB Yaghan Basin, OB Ona Basin, PAR: Phoenix Antarctic Ridge, SFZ: Shackleton Fracture Zone, WSR: West Scotia Ridge, OSD: Ona Sea floor Depression,.

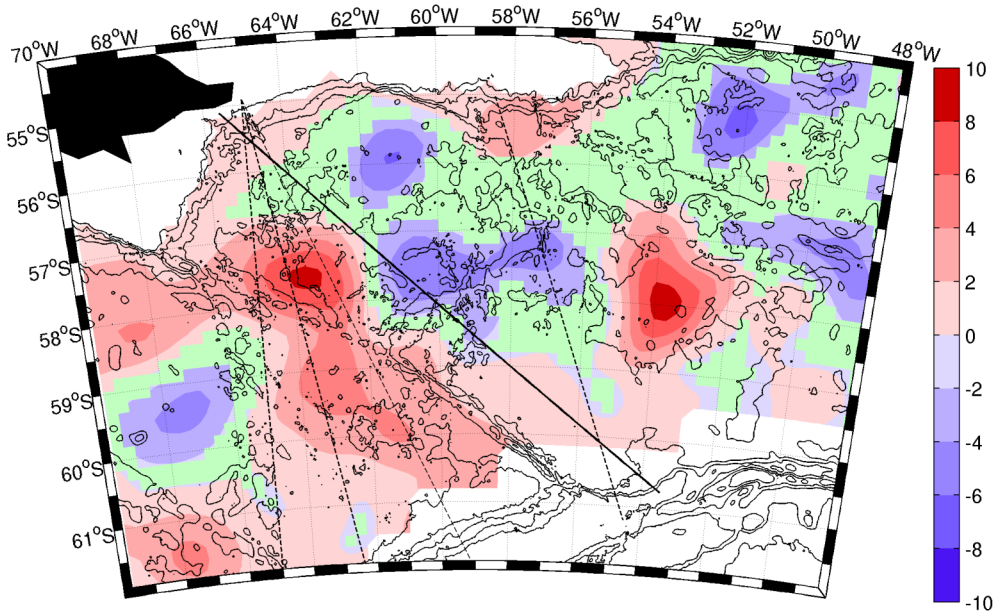

Figure 2: Linear trends in dynamic topography (mm per year) from January 1993 to December 2009. The significance of the trend was computed using a two-sided Student t-test with a confidence limit of 99%. Areas where the trend is not significant are colored in green. White areas correspond to the regions where the time series are incomplete and the data from over the continental slope (depth less than 500 m) are disregarded. Black contours represent the bathymetry between 4000 m and 1000m with contour intervals of 500 m. The black diagonal line indicates the Jason track 104. Black dashed lines represent XBT surveys from the US Antarctic supply vessel (west of track 104) and the repeat hydrographic section SR1b (east of track 104). (updated from Barré et al, 2011).

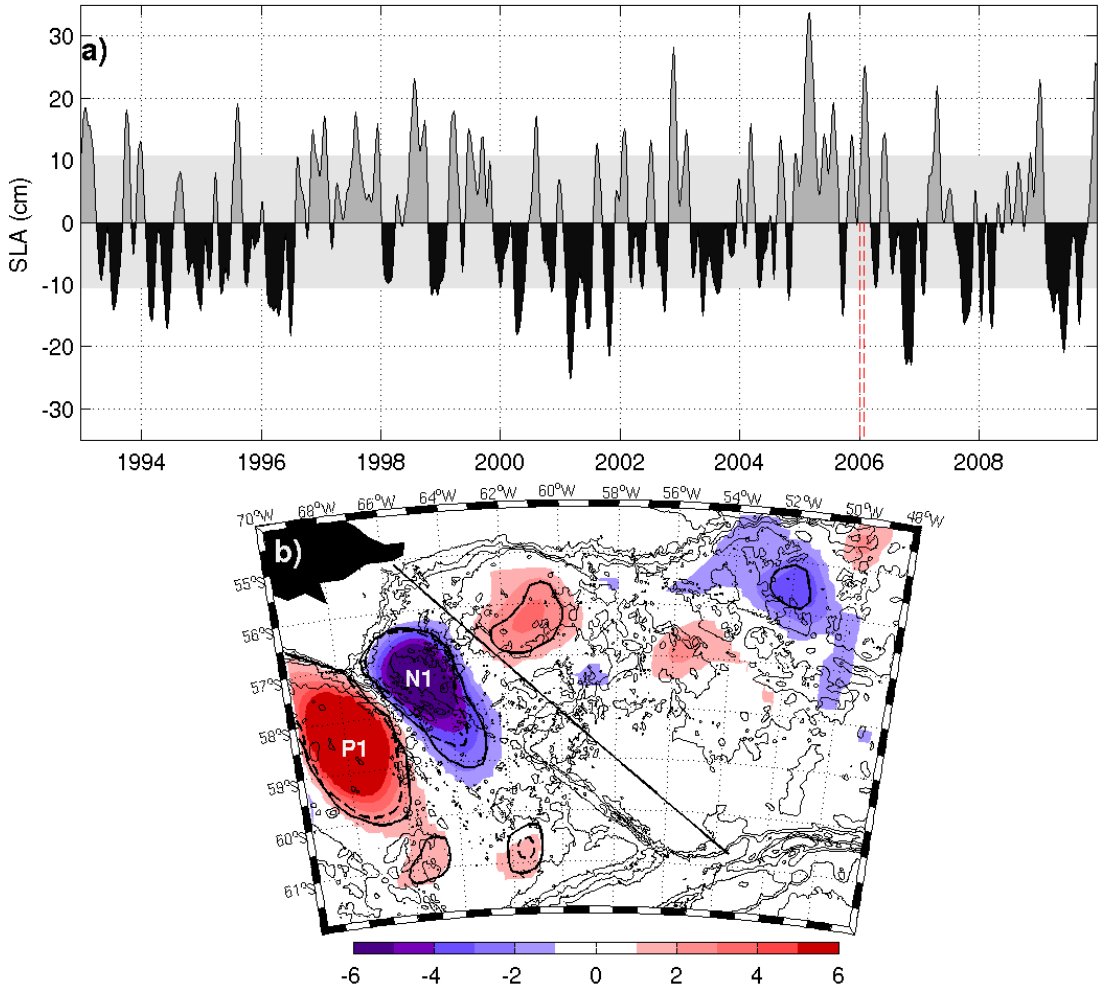

Figure 3:

a Time series of sea level anomaly (SLA) over a 1°x1° box centered at 68°W and 58.5°S (location P1). The linear trend has been removed.

b Regression of SLA, in Drake Passage, on the normalized time-series in Fig.3a. Solid black contours represent the correlation at the 90% confidence level; dashed black contours represent the 95% confidence level. The regression map suggests that the strong anomaly (P1) on the western side of the PAR can be associated with an anomaly of the opposite sign (N1) on the eastern side of the PAR. Thin black lines are bathymetry isobaths (2000, 3000 and 4000m). (updated from Barré et al., 2011)

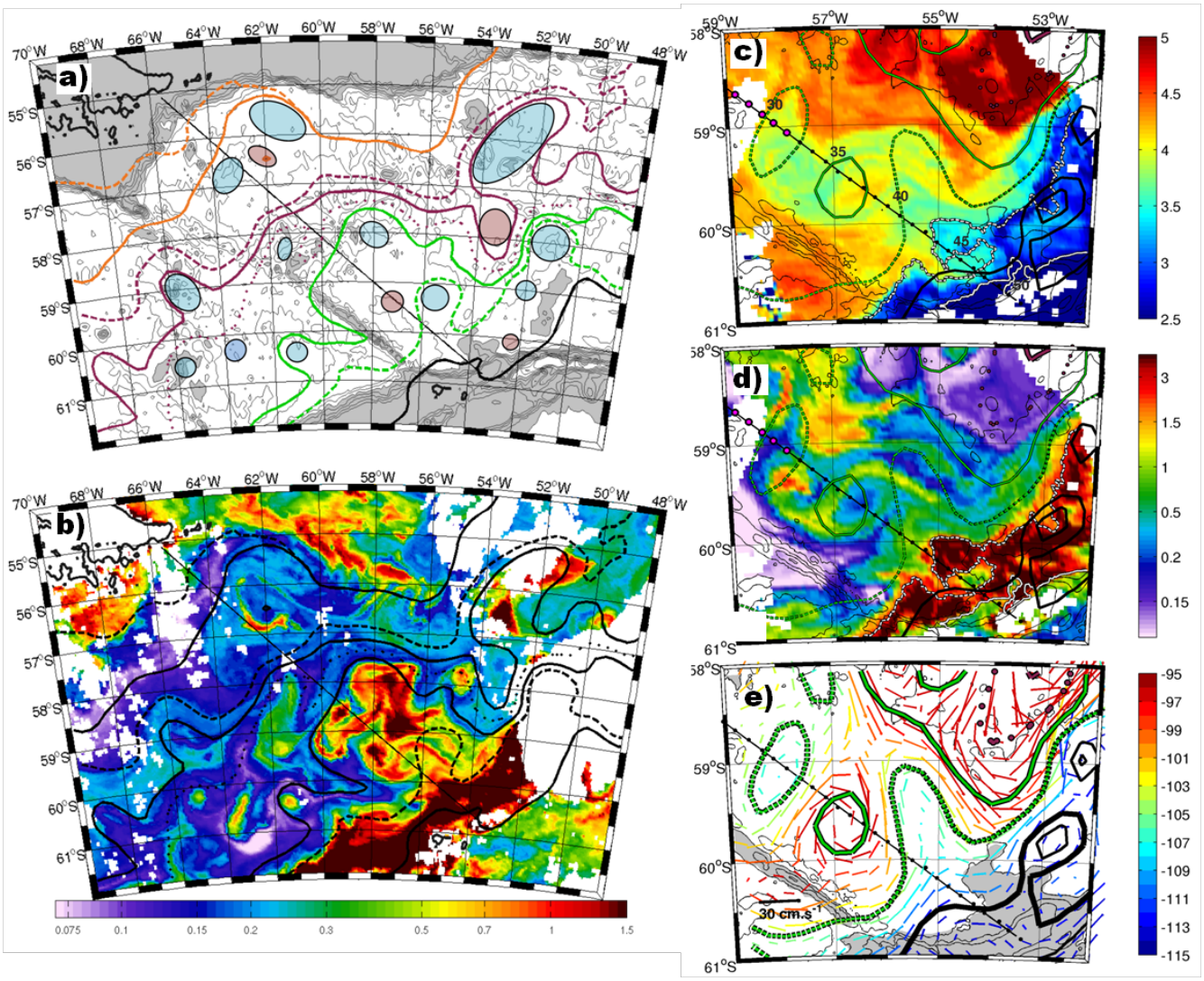

Figure 4:

a Schematic of the frontal branch and eddy location during the ANT-XXIII/3 cruise period derived from altimetry (composite map from 15 to 21 January 2006). SAF branches in orange; PF branches in purple; SACCF branches in green; and SB, in black. Blue patches are the major cyclonic eddies and red patches are the major anticyclonic eddies.

b One-week (17-24 January 2006) composite image of chlorophyll-a concentration (mg.m-3) from MODIS. Black contours are the branches of the ACC fronts and eddies like in a.

c, d, e :Satellite views of the Ona Basin late January 2006:

c: Sea surface temperature (°C) from 22 January 2006 (MODIS). Superimposed are the front and eddy locations derived from the 7-day composite altimetry map centered on January 25: PF-S (purple dotted line); SACCF-N (green solid line), SACCF-S (green dashed line); and SB (black line). The white dotted line is the 2.36 mg.m-3 isoline in Chlorophyll-a concentration and the continuous white line the northern limit to surface waters colder than 2.3°C.

d: Chlorophyll-a concentration (mg.m-3) from 22 January 2006 (MODIS). Contours like in c.

e: Surface geostrophic velocity field derived from the 7-day composite map of altimetric absolute dynamic topography centered on January 25. The color code indicates absolute dynamic topography values (in centimeters). Schematics of the front and eddy locations correspond to the date of the map (same color code as in c and d).

On all maps, thin black contours represent the bathymetry between 4000m and 1000m with contour intervals of 500m. Bottom depths shallower than 3000 m are shaded in grey. The black diagonal line indicates the Jason track 104. (adapted from Provost et al., 2011)

The OVIDE Project
Documenting and understanding the inter annual to decadal variability of the North Atlantic Subpolar gyre

Herlé Mercier, Pascale Lherminier, Nathalie Daniault, Virginie Thierry, Bruno Ferron, Thierry Huck
Laboratoire de Physique des Océans, CNRS, Ifremer, IRD, UBO, Plouzané, France

Since 2002, the Ovide project occupies every other year, in June-July, the A25 hydrographic section between the southern tip of Greenland at 60°N and Portugal at 40°N (Figure 1). This is a repeat of a line that was previously occupied during the International Geophysical year and, in the framework of the Fourex project, in September 1997. The Ovide project is a contribution to CLIVAR. During each cruise, CTDO2 and L-ADCP measurements are conducted from the surface down to the sea-floor at about 95 hydrographic stations and VM-ADCP is running during all cruises. Nutrients, CFCs, pH and alkalinity are measured from water samples obtained from the 28 bottle rosette. The Ovide cruises also contributes to maintaining the Argo array by deploying ~15 floats during each cruise. The cruises are a collaborative work with P. Morin (station biologique de Roscoff, France) and A. Rios and F. Perez (IIM Vigo, Spain). We summarize below one of the results obtained from the analysis of the Ovide data set that was complemented by a reanalysis of Fourex.

For the first time in the subpolar North Atlantic, a large variability in the amplitude of the meridional overturning circulation (MOC) and the associated heat flux (HF) has been documented. Estimates are based on an inverse model analysis of the Ovide and Fourex hydrographic sections (Lherminier et al., 2007, Lherminier et al. 2010, Gourcuff et al. 2011). Figure 2 shows that across the Fourex/Ovide hydrographic section the main balance in terms of transport is between the North Atlantic Current (NAC, $\sigma 1 < 32.1$), east of the subarctic front (SAF) and the net transport of dense water ($\sigma 1 > 32.1$) west of the SAF. This balance defines the MOC and shows that the NAC transport variability is a good proxy of the MOC variability. Focussing now on the MOC, the maximum amplitudes were observed in September 1997 (19 Sv and 0.69 PW for the MOC and the HF, respectively) and the minimum amplitudes were observed in June 2006 (11 Sv and 0.29 PW for the MOC and the HF). Values for 2002, 2004 and 2008 are in between. Although it is tempting to relate the decrease in the MOC amplitude between Fourex and Ovide 2006 to the spin-down of the subpolar gyre that has been reported by Hakkinen and Rhines (2009), it should be stressed here that those measurements quantify the variability of the MOC and associated heat flux but the associated time scales have still to be determined. For instance, Daniault et al. (2011) showed from an analysis of a current meter array in the East Greenland Irminger Current that at the time of the Ovide 2006 the transport of this current, which is an essential component of the MOC, reached a minimum that lasted for a few weeks, associated with a relatively weak wind stress curl in the Irminger Gyre (as compared to the 20-year average).

Références

Daniault, N., P. Lherminier, H. Mercier, 2011: Circulation and transport at the south east tip of Greenland. J. Phys. Oceanogr., in press.

Gourcuff, C., P. Lherminier, H. Mercier, P. Y. LeTraon, 2011: Altimetry combined with hydrography for ocean transport estimation. J. Atmosph. Ocean. Tech., submitted.

Hakkinen, S., P. Rhines, 2004: Decline of the subpolar North Atlantic Circulation during the 1990's. Science, 304, 555-559.

Lherminier, P., H. Mercier, C. Gourcuff, M. Alvarez, S. Bacon, C. Kermabon, 2007: Transports across the 2002 Greenland-Portugal Ovide section and comparison with 1997. J. Geophys. Res. Oceans., 112, C07003, doi:10.1029/2006JC003716.

Lherminier, P. H. Mercier, T. Huck, C. Gourcuff, F. F. Perez, P. Morin, A. Sarafanov, 2010: The Atlantic Meridional Overturning Circulation and the subpolar gyre observed at the A25-OVIDE section in June 2002 and 2004. Deep Sea Res. I, doi:10.1016/j.dsr.2010.07.009.

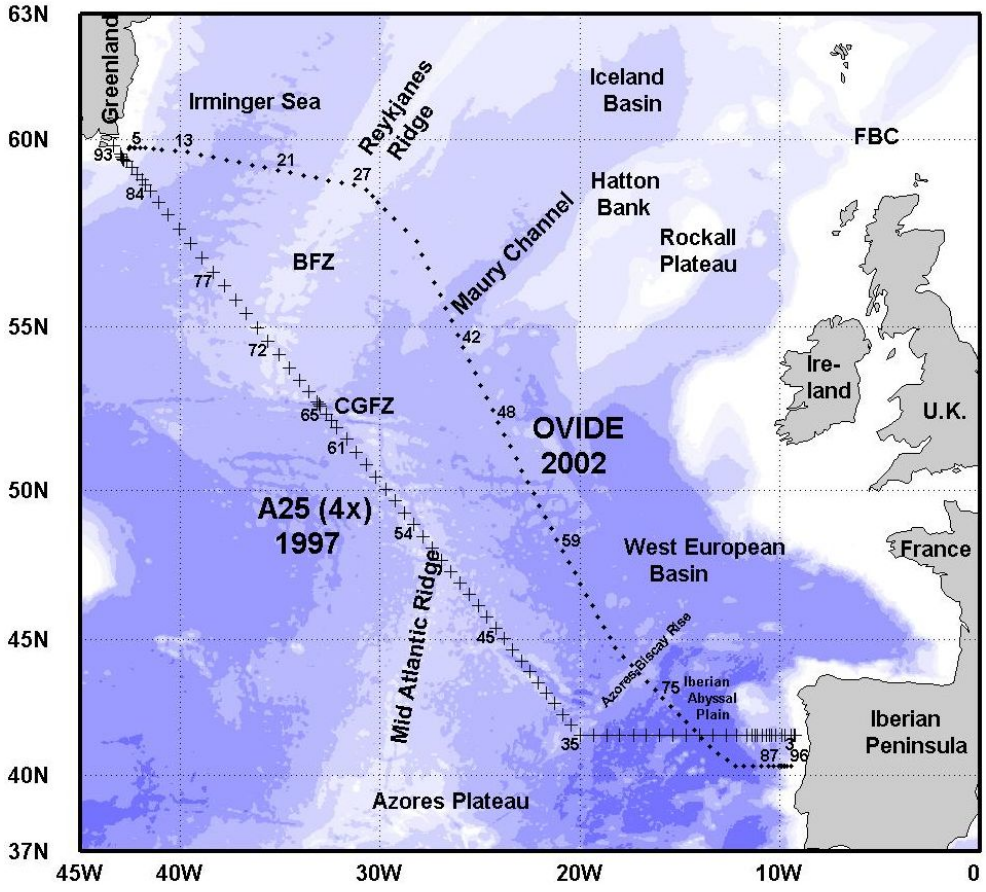

Figure 1: The Fourex (1997) and the Ovide (2002, 2004, 2006, 2008, 2010) hydrographic lines

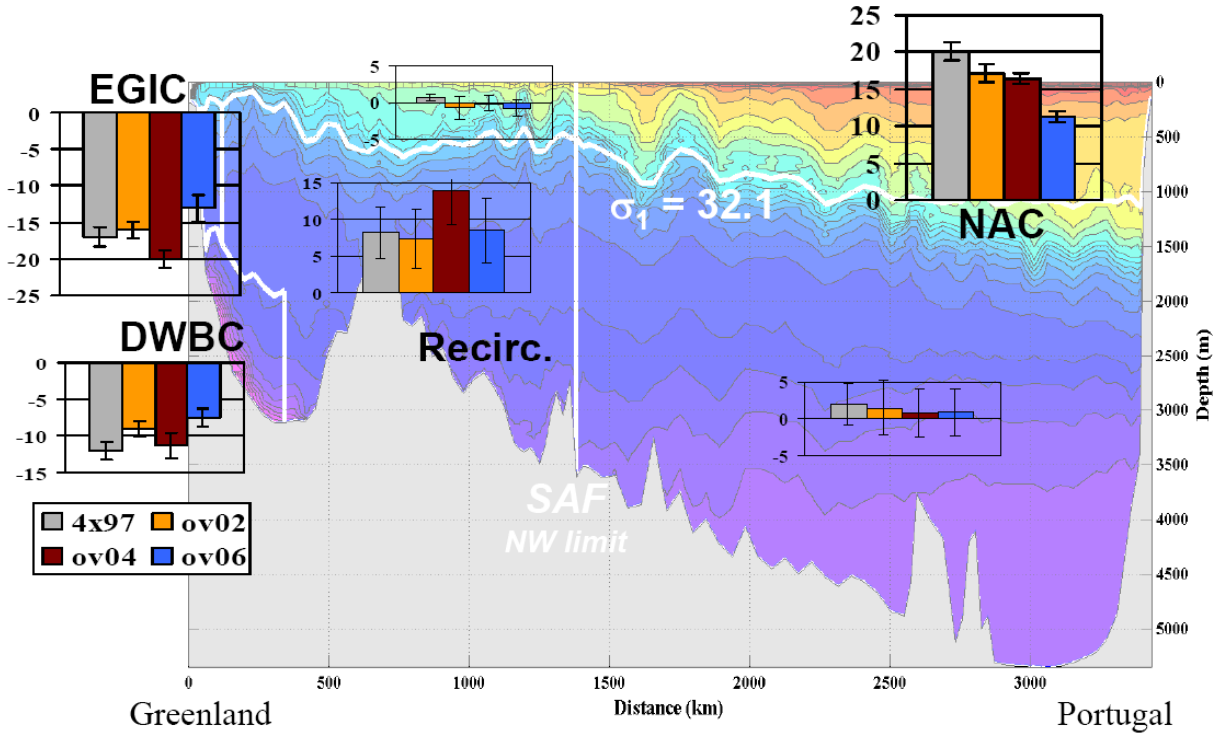

Figure 2 : Transport variability in Sv (1 Sv = 106 m3 s-1) contributing to the MOC obtained from an inverse model analysis of Fourex (1997) and OVIDE (2002, 2004, 2006) hydrographic sections. Northward transports are positive. EGIC : East-Greenland Irminger Current ; DWBC : Deep Western Bourndary Current ; Recirc. : Deep recirculation in the Island basin and the eastern Irminger Sea; NAC: North Atlantic Current. SAF: Sub-arctic front. The σ1 = 32.1 isopycnal is the limit between the upper and lower limbs of the MOC.

MESOSCALE AND SUBMESOSCALE TURBULENCE

Patrice Klein (LPO, Plouzané, France) and Guillaume Lapeyre (LMD, Paris, France)

The first 500-1000m of the upper ocean have been known for many years to be crucial for the biogeochemical and the atmosphere-ocean coupling systems. At the end of the 20th century, data from conventional satellite altimeters (that capture O(100km) structures) and global-scale oceanic simulations with a 10km resolution have unveiled the strong turbulent character of the mesoscale eddy field in many oceanic regions. These oceanic mesoscale eddies (the ocean weather system), characterized by horizontal scales of O(100km) and depths between 500m and 1000m constitute the dominant part of the total kinetic energy and are known to significantly contribute to the lateral transport of heat, momentum and tracers (Ferrari and Wunsch, ARFM, 2009) and to the biogeochemical system (McGillicuddy, GGC, 2003).

Since 2005 a bunch of studies, both numerical and experimental, have profoundly changed our « turbulent » vision of the upper oceanic layers. They reveal the importance of submesoscales (such as filaments with a 10km width and small-scale vortices with a 5-40km diameter) that are ubiquitous on the Sea Surface Temperature (SST) and Ocean Color images but whose dynamical impacts were totally ignored before. Dynamics of the first 500m of the ocean can now be viewed as captured by a sea of interacting mesoscale eddies and submesoscale structures (Klein et al., JPO, 2008, Capet et al., JPO, 2008, Klein and Lapeyre, ARMS, 2009). These new studies have offered an unprecedented insight on the dramatic impact of these submesoscales. These submesoscales are associated with vertical velocities that can reach 100m/day (typically one order of magnitude larger than those associated with mesoscale eddies) down to 200-500m below the surface (Legal et al., JPO, 2007; Nagai et al., JGR 2006; Klein et al., JPO, 2008; Capet et al., JPO, 2008). As a consequence they impact much more significantly, than previously thought, the global ocean circulation and the biogeochemical system. Such new insight has been made possible because of the development of instruments mounted on towed vehicles, new float devices in the upper layer but, principally, because of the fast development of supercomputers.

Quantification on a global scale indicates that, in oceanic regions overcrowded with mesoscale eddies such as in the Gulf Stream, the Kuroshio and the Antartic Circumpolar Current, the vertical velocity field associated with submesoscales represent almost 70% of the total vertical velocity field (Lapeyre and Klein, JMR, 2006; Klein et al., JPO, 2008). The remaining 30% being located inside mesoscale eddies. As a result submesoscales explain more than 60% of the total nutrient vertical fluxes. This may provide an answer to the ongoing debate about which physical processes can close the nutrient balance in the ocean (McGillicuddy, GGC, 2003). Furthermore the presence of submesoscales make the primary production in the ocean to be multiplied by a factor 2 (Levy, 2005; Martin et al., GGC, 2006; Klein and Lapeyre, ARMS, 2009). High resolution primitive equation simulations (1km) in large domain performed on the Earth simulator have unveiled the impact of submesoscales on the ocean dynamics at larger scales. Kinetic energy associated with these submesoscales is globally smaller than that associated with mesoscale eddies but their presence explains that the mesoscale kinetic energy is multiplied by a factor 2 (Klein et al., JPO, 2008; and Capet et al., JPO, 2008) and that the sea surface temperature increase by almost 1o K (due to ageostrophic motions) (Klein et al., JPO, 2008)! Roullet and Klein (PRL, 2010) further point out that the submesoscales accelerates the ocean energy circuit – between potential and kinetic energy among the different (large and small) scales - through the vertical velocity field.

The physics that explains the importance of submesoscales in the upper ocean is frontogenesis (the same mechanism that drives atmospheric fronts): density anomalies are stretched by mesoscale eddies into small-scale elongated patterns which increases the density gradient they are associated with and triggers frontogenesis. The resulting vertical velocity field affects the first 500m and provides a pathway between the surface boundary layer (or the surface mixed-layer) and the ocean interior. These submesoscales are part of a surface dynamical mode, first introduced by Blumen (JAS, 1978), extended to the ocean by Held et al. (JFM,1995) and Lapeyre and Klein (JPO, 2006) and to the atmosphere by Hakim et al. (JAS, 2002) and Tulloch and Smith (JAS, 2009). This mesoscale/submesoscale turbulence in the upper ocean is driven by the surface potential vorticity (that can be estimated from the Sea Surface Height) and by the interior potential vorticity (Lapeyre and Klein, JPO, 2006). The high resolution simulations performed by the French scientists on the Earth Simulator and by the UCLA scientists have provided unvaluable insights on the importance of this mesoscale/submesoscale turbulence. Global observations of the dynamics this mesoscale/submesoscale turbulence are presently lacking but are highly needed to constrain future realistic numerical simulations at these resolutions. Sea Surface Temperature and Ocean Color satellites images have such a high resolution but they are much affected by the clouds and, when available, do not provide any dynamical information. Future satellite altimeter missions (such as the Surface Water and Ocean Topography (SWOT) mission, see Fu and Ferrari, EOS, 2009) should allow to get dynamical information at the ocean surface at a resolution ten times higher than the conventional altimeters and, therefore, reduce the gap between numerical and data resolutions. But one major challenge is how to exploit the full potential information

provided by these new high resolution satellite data - when combined with existing data (such as the Global Argo float database- to retrieve and diagnose these new dynamical impacts related to the submesoscales in particular those related to the vertical velocity field in the first 500m and to the air-sea fluxes. This is one of the major challenge of the present decade.

A global numerical model to study the interannual variability of the ocean

Anne Marie Treguier, CNRS
Laboratoire de Physique des Oceans, UMR 6523 CNRS-IFREMER-IRD-UBO, IUEM

The DRAKKAR project is a collaboration between French research laboratories (LEGI, Grenoble; LPO, Brest; LOCEAN, Paris), Mercator-Ocean, and other teams in Europe (Southampton, U.K; Kiel, Germany) and Canada. In 2006-2010 a global ocean and sea ice model has been developed, based on the NEMO platform (www.nemo-ocean.eu), with a ¼° resolution: a grid scale ranging from 27 km at the equator to an average of 12 km in the Arctic ocean. A new representation of bottom topography and numerical schemes have brought improvements in the representation of the main current systems and the associated eddies (Barnier et al, 2006; figure 1). Simulations of the ocean variability over the past decades (1958-2007) have been performed, forced by atmospheric data based on ECMWF reanalysis and analyses (Brodeau et al, 2010). The results of these simulations have been distributed to a wide international community. Variability mechanisms have been analyzed globally or regionally (in the Arctic, the Mediterranean sea, the Southern Ocean, the North Atlantic…). Only two examples are given here.

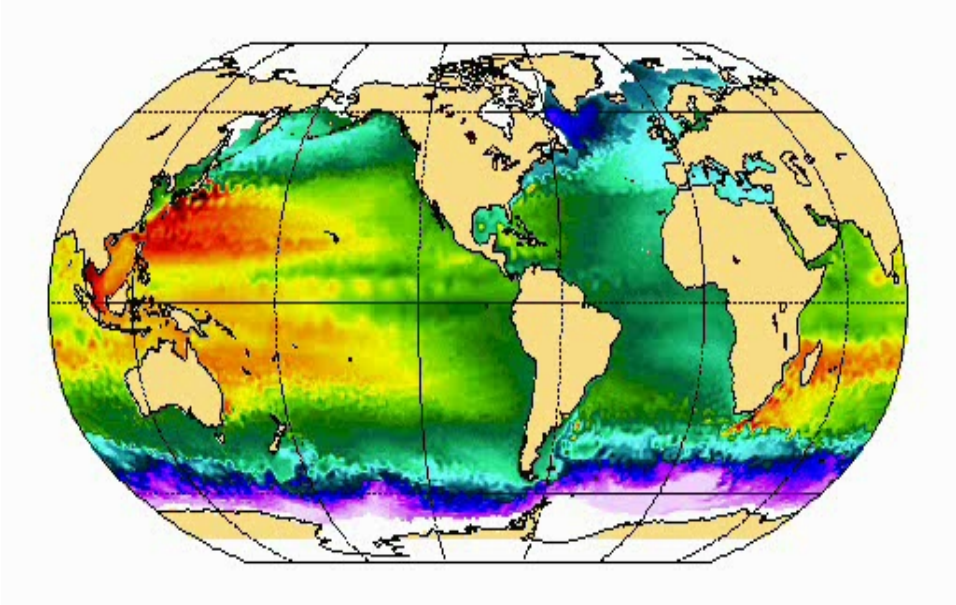

Figure 1: Map of a 5-day average of sea level in the DRAKKAR ¼° model (the ice cover is indicated in white). The model reproduces well some eddying regions like the Agulhas retroflection or the Zapiola Anticyclone south of the Brazil-Malvinas confluence zone. The ¼° resolution is still too coarse in other areas, for example in the Gulf stream, the Kuroshio, or west of Australia in the Indian Ocean

Mechanisms of regional sea level trends (1993-2001).

Lombard et al (2008) have compared the trend in sea level in DRAKKAR simulations and observations. The good agreement (figure 2) allows to use the model to analyse the possible causes of the observed trends. The model (which has no assimilation of satellite nor in situ data) demonstrates that regional changes in sea level over that period are largely forced by the atmosphere. They are mainly due to thermosteric changes in the upper 750m. Wind stress trends over that period explain some of the sea level trends, especially in the tropical Pacific and Indian Ocean.

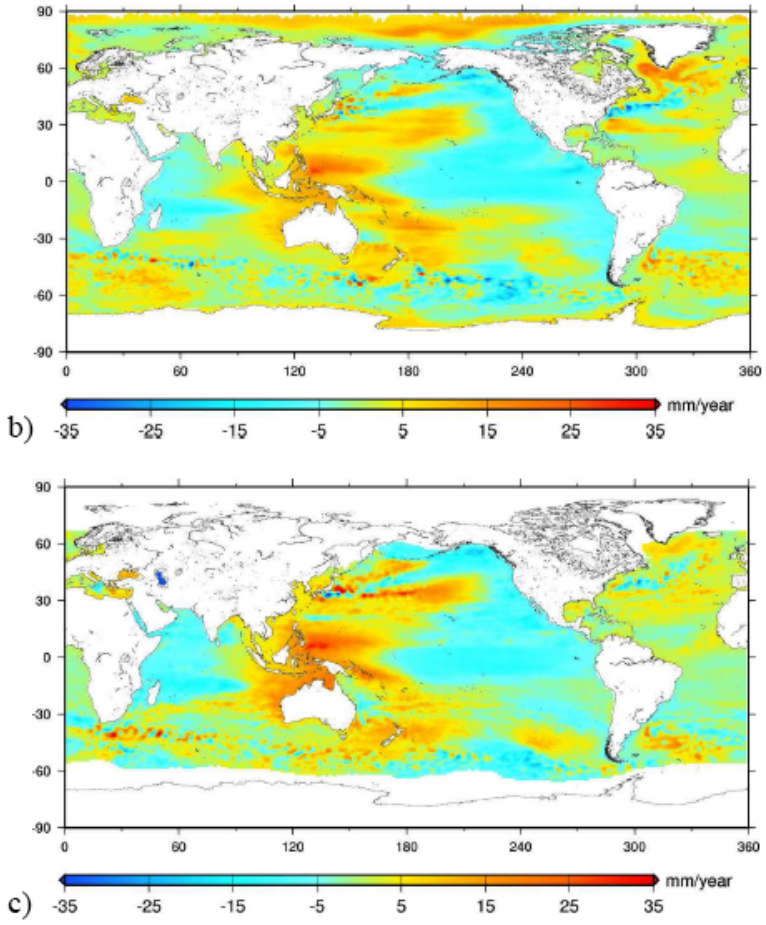

Figure 2: Regional trends of sea level between 1993 and 2001 (mm/year). Top: ORCA025; bottom: observation by satellite altimetry. From Lombard et al, 2008.

Ice and freshwater transport variability along both sides of Greenland

The ¼° global DRAKKAR model simulates the variability of the Arctic Ocean and its interaction with the Pacific and Atlantic Oceans, with a mesh fine enough to resolve Bering Strait and the main pathways through the Canadian Archipelago. The model allows to propose a quantitative estimate of the liquid freshwater and ice fluxes from the Arctic to the Atlantic (Lique et al, 2009; figure 3). Regarding the mechanisms of interannual variability, the model suggests a striking difference between both sides of Greenland. At Davis Strait to the west, the variability is due to the volume transport, while on the east side at Fram Strait, the variability is due in equal parts to the variations of the volume transport and to variations of the salinity, linked with interannual variability of the ice-ocean exchanges north of Fram Strait.

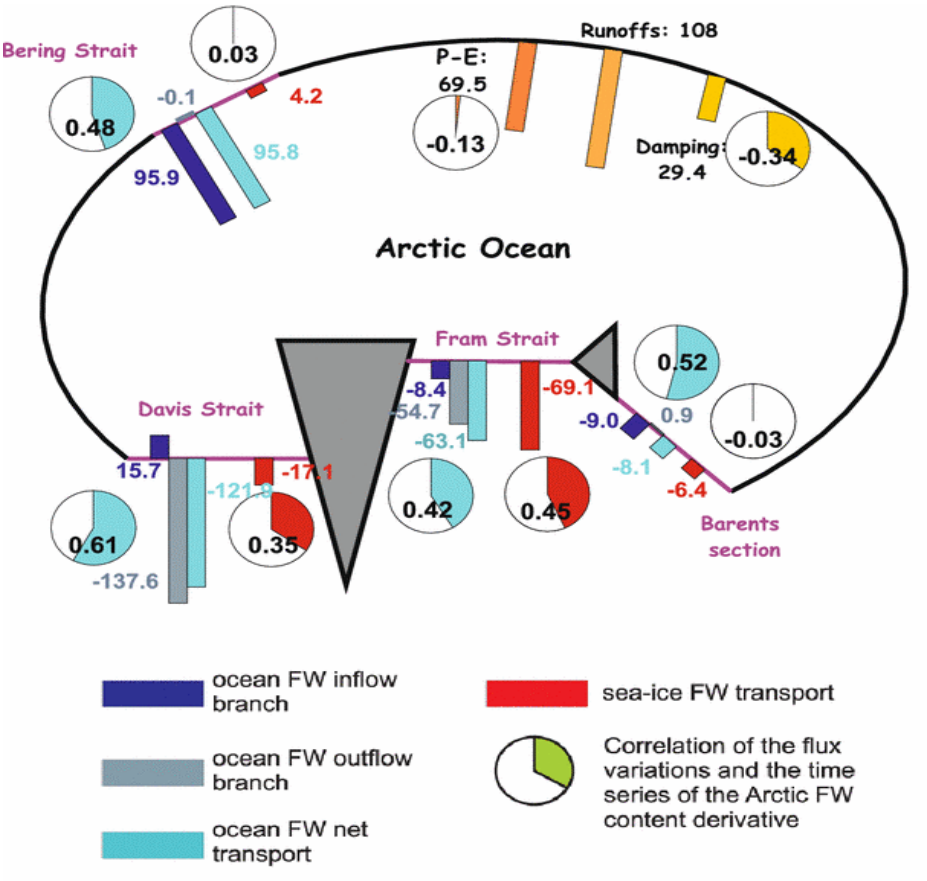

Figure 3 (Lique et al, 2009). Schematic view of the Arctic freshwater balance. Mean value of each source and sink is represented (bar, in mSv), as well as the correlation of its variations with the times series of the Arctic freshwater content derivative (circular diagrams). The sign of the freshwater

fluxes indicates if the flux represents a sink or a source of freshwater for the Arctic Ocean, regardless the direction of the volume fluxes (For instance, the inflow branch through Fram Strait brings waters with salinity higher than 34.8, and thus has a negative sign)

Barnier B., G. Madec, T. Penduff, J.-M. Molines, A.-M. Treguier, J. Le Sommer, A. Beckmann, A. Biastoch, C. Böning, J. Dengg, C. Derval, E. Durand, S. Gulev, E. Remy, C. Talandier, S. Theetten, M. Maltrud, J. McClean, and B. De Cuevas, 2006: Impact of partial steps and momentum advection schemes in a global ocean circulation model at eddy permitting resolution. Ocean Dynamics, Vol 4, DOI 10.1007/s10236-006-0082-1.

Brodeau, L., B. Barnier, A.M. Treguier, T. Penduff, S. Gulev, 2009: An ERA40-based atmospheric forcing for global ocean circulation models. Ocean Modelling, 31, 88-104, doi: 10.1016/j.ocemod.2009.10.005

Lombard, A., G. Garric, and T. Penduff, 2009 : «Regional patterns of observed sea level change: Insights from a 1/4° global ocean/sea-ice hindcast ». Ocean Dynamics, 59, 3, 433-449.

Lique, C., Treguier, A.M., Scheinert, M., Penduff, T., 2009: A model-based study of ice and freshwater transport variabilities along both sides of Greenland. Climate Dynamics, 33 (5), 685-705, DOI: 10.1007/s00382-008-0510-7.

Inter-decadal modulation of ENSO nonlinearity and its evolution in a warming climate

Boucharel J. (1), Dewitte B. (1) (2), du Penhoat Y. (1) (2), Garel B. (3), Yeh, S.-W. (4), Kug J.-S. (5)
(1) Université de Toulouse; UPS (OMP-PCA); LEGOS, 14 Av. Edouard Belin, F-31400 Toulouse, France.
(2) IRD; LEGOS, F-31400 Toulouse, France.
(3) Université de Toulouse; INP-ENSEEIHT, Institut de Mathématiques de Toulouse (UPS) France.
(4) Department of Environmental Marine Science, Hanyang University, Ansan, South Korea
(5) Korea Ocean Research and Development Institute, Ansan, South Korea.

1. Introduction

El Niño Southern Oscillation (ENSO) is the dominant mode of tropical climate variability, whose variations influence climate and ecosystems as well as many societies around the globe. It is therefore of great interest to understand its past, present and future variations. Over the last century, ENSO properties including amplitude, frequency and propagating features underwent significant changes at decadal to interdecadal timescales (An, 2004), which are partly revealed by the presence of climate shifts (Guilderson and Schrag, 1998) within ENSO typical timeseries. For instance, the two decades after the 1976/77 climate shift were characterised by more frequent and stronger El Niño events compared to previous decades (An and Wang, 2000; An, 2004; Moon et al., 2004). These changes in ENSO characteristics are intimately linked to changes in the mean state of the tropical Pacific because the dominant feedback processes associated with ENSO, namely the zonal advective and thermocline feedbacks, depend explicitly on the zonal mean Sea Surface Temperature (SST) and thermocline gradients, respectively (Zebiak and Cane, 1987; An and Jin, 2001).

Another recently documented characteristic of ENSO is its asymmetry, which reflects the nonlinearity of the tropical Pacific system (An and Jin, 2004). ENSO asymmetry also fluctuates over decadal to interdecadal timescales that are related to changes in mean state (Rodgers et al, 2004; Dewitte et al., 2007). In particular, the latter can result from the residual effect of the ENSO asymmetry variability (Schopf and Burgman, 2006; Dewitte et al., 2007), potentially leading to a tropical Pacific natural coupled mode over decadal timescales (Choi et al., 2009).

Because of this complex interaction between mean state and ENSO at a wide range of frequencies, it is difficult to provide an unambiguous explanation for the impact of global warming on ENSO. As a matter of fact, the current generation of models exhibits a wide range of behaviours with regards to their sensitivity to global warming (Guilyardi et al., 2009). In particular, the evolution of tropical Pacific SST, especially the mean zonal equatorial gradient remains a noteworthy source of uncertainty (DiNezio et al., 2009).

Recently, Yeh et al. (2009) showed, with a group of IPCC models, that most consistent changes in ENSO characteristics due to global warming take place in the central equatorial Pacific (i.e. the Niño4 region (150°E-150°W; 5°S-5°N)). They showed that global warming leads to increased SST variability over the central tropical Pacific in the form of an increased occurrence of the so-called Modoki or Central Pacific (CP) El Niño (Ashok et al., 2007) relatively to the traditional so-called Eastern Pacific (EP) El Niño characterized by positive SST departure from normal in the Niño3 region (150°W-90°W; 5°S-5°N).

In this study, we further examine the relationships between changes in mean state and changes in ENSO properties, especially El Niño flavours and the importance of associated nonlinear mechanisms through an alternative statistical measure. These analyses are carried out on both reconstructed historical datasets and CGCMs outputs.

2. Statistical diagnosis of ENSO nonlinearity

Whereas ENSO nonlinearity has usually been considered through its asymmetric character (in particular as El Niño events are stronger and more numerous than La Niña's), recent studies indicate that ENSO also has a signature on higher-order statistical moments (Timmermann, 1999). This tends to emphasize the highly nonlinear nature of the tropical Pacific system and calls for the use of statistical tools that can effectively measure ENSO nonlinearity.

We propose here an alternative to classic Gaussian statistics, namely the □-stable laws, to explicitly consider 2 main features of the ENSO Probability Density Function (PDF) (Figure 1): the asymmetry and the weight of the distribution tail associated with warm strong El Niño episodes.

In brief, non-Gaussian α-stable laws, (heavy tailed laws) are characterized by four main parameters. The main ones, $0 < \alpha \leq 2$ and $-1 \leq \beta \leq 1$, respectively allow to diagnose the "non-Gaussian degree" (the PDF tails weight) and the asymmetry (~ skewness) of the set to be measured. Simply put, the analyses of these two parameters allow measuring the deviation of a distribution from a Normal law; this deviation being representative of the underlying nonlinear processes. When $\alpha = 2$ and $\beta = 0$, the result is a Gaussian law. The lower α, the more α-stable the distribution and the more nonlinear the associated mechanisms. See Mandelbrot (1963) and Boucharel et al. (2009) for a more complete

description. It is noteworthy that the measurement of nonlinearity through the α parameter does not discriminate between nonlinear processes. Actually, the sources of nonlinearities of the tropical Pacific system remain numerous ranging from turbulent and ocean-mixing processes in the form of tropical instability waves for instance, to high frequency atmospheric forcing (An, 2009).

Koutrouvelis (1980) proposed a trustful regression method to estimate α-stable laws parameters.

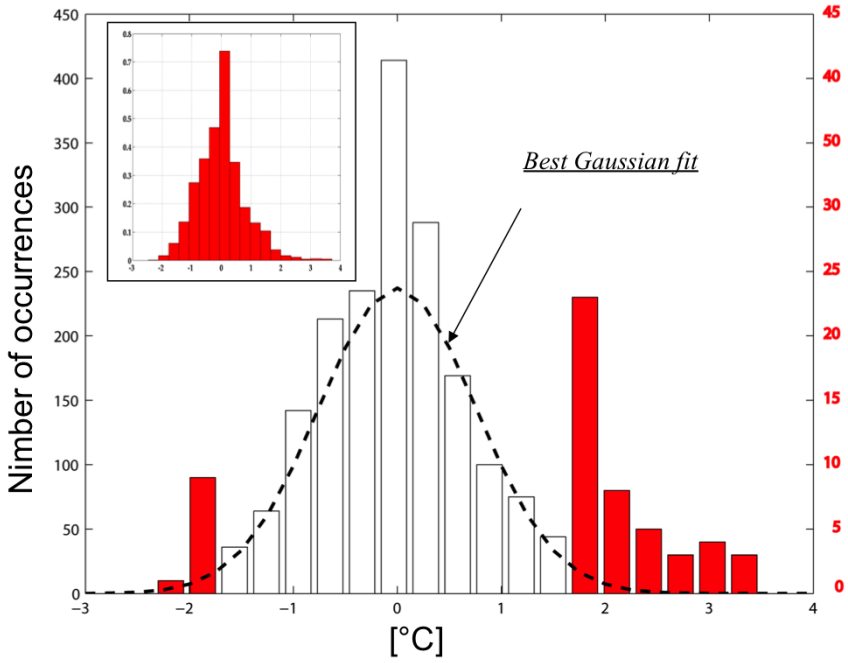

Figure 1. Histogram of Niño3 SST anomalies from Kaplan et al. (1998) reconstructed dataset. The y-axis of red bars (events greater than standard deviation) has ten times increased scale. Normalized histogram I the upper left quadrant.

3. Inter-decadal modulation of ENSO nonlinearity (statistics).

Over the inter-shift periods detected in Boucharel et al. (2009) (statistically confident ruptures detected in 1903, 1976 and 1998 through a bivariate test elaborated by Maronna and Yohai, 1978), the results of the estimation of □ and □ on distinct warm/cool periods (Figure 2) indicate that the ENSO statistics experienced significant changes. In particular, warm periods were characterised by stronger asymmetry and a greater deviation from Gaussianity (smaller α and □ ~ 1) whereas the cool period exhibited a Gaussian symmetrical pattern on average over the tropical Pacific (α ≈ 2 and □ ~ 0). A comparable tendency was found in the intermediate complexity Zebiak and Cane (ZC) model. In particular the ZC model had increased (reduced) nonlinearity quantified through nonlinear advection within the mixed layer (Nonlinear Dynamical Heating (NDH)) during warm (cool) periods (An and Jin, 2004; Boucharel et al., 2009). Consistently with recent studies, nonlinear dynamics is found to be responsible for rectification of ENSO variability through changes in ocean background. Although current measures of ENSO nonlinearities (through NDH) have provided meaningful information on the rectification of ENSO variability by changes in mean state, they may not fully account for the complexity of the rectified effect.

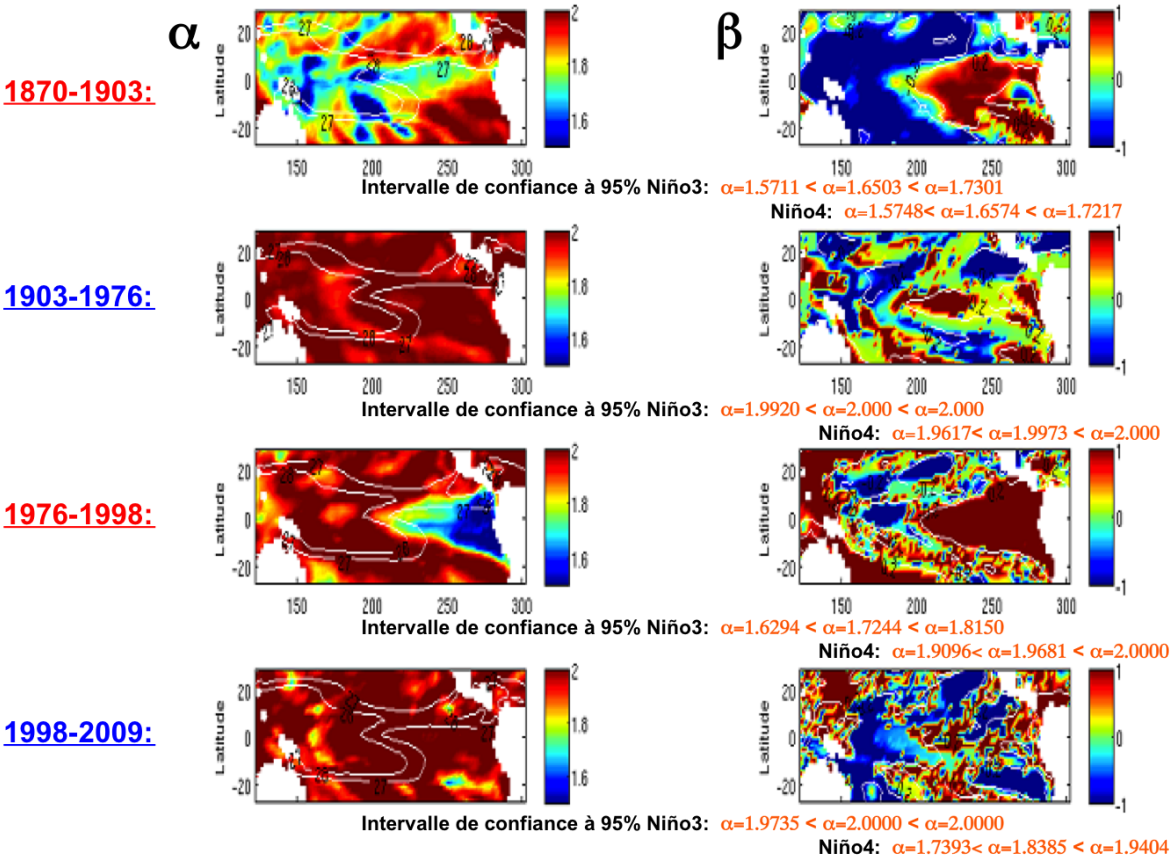

Figure 2. □ and □ parameters on distinct warm (1870-1903 and 1976-1998) and cool (1903-1976 and 1998-2009) inter-shifts periods estimated from Kaplan et al. (1998) reconstructed dataset. Confidence intervals for parameters estimation on Niño3 and Niño4 indices are provided below each plot.

In order to test further the relationships between ENSO nonlinearity and the tropical Pacific mean state, we took advantage of the CMIP3 Coupled General Circulation Models (CGCMs) database and the different scenario experiments provided by the fourth version of the assessment report of the IPCC. We selected a set of models available through the CMIP3-IPCC-AR4 data centre at the Program for Climate Model Diagnosis and Intercomparison (PCMDI) and tested them in different configurations in terms of greenhouse gases concentration (respectively the Pre-Industrial reference -PICTRL-, the doubling -2xCO2- and quadrupling -4xCO2- greenhouse gases concentration). In particular, since the focus of the study deals with the diagnostic of high-order statistics and their response to changes in mean state, we followed the classification established in Table 5 in Boucharel et al. (2009). The latter evaluates the performances of the whole CMIP3 database in simulating irregular (nonlinear, □-stable) ENSO timeseries along with a noteworthy low frequency modulation of the tropical Pacific mean state (revealed by the presence of climate shifts). Interestingly, models able to represent a significant decadal to inter-decadal variability are also strongly nonlinear (with regards to the α parameter analysis). These models (in bold in Table 5 in Boucharel et al. (2009)) will be the models of interest in the present study. Interestingly, this "nonlinear" classification is consistent with other recent studies dedicated to intercomparison (Belmadani et al., 2010 among others).

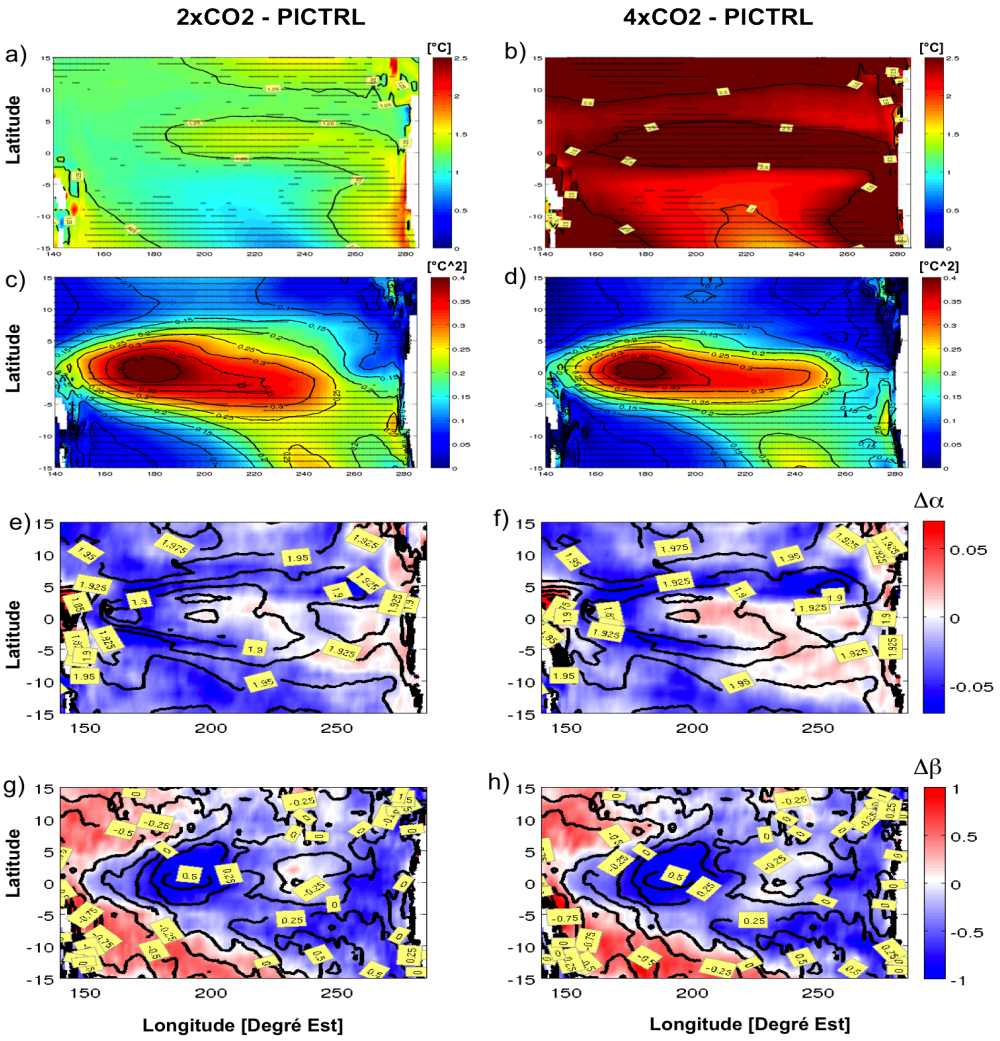

Figure 3. Changes in tropical Pacific statistics between different IPCC scenarios for the multi model ensemble mean (2xCO2 – PICTRL on left panels and 4xCO2 – PICTRL on right panels). Changes in: mean SST a) and b), RMS SST c) and d). Dots denote 95% statistical confidence level based on a Student's t-test. Changes in: □parameter e) and f), □ parameter g) and h). Contours in e), f), g) and h) panels denote □ and □ parameters values for the multi models mean for the PICTRL experiment.

Figure 3 displays the change in mean state for the model ensemble mean considered in this study for the $2xCO_2$ and $4xCO_2$ scenario. It consists of an El Niño-like pattern (i.e. maximum mean SST changes over the Cold Tongue region, Figure 3a). Interestingly, for the $4xCO_2$ scenario, models simulate an enhanced equatorial warming (Figure 3b), rather than an El Niño-like warming. These changes in mean SST are associated with changes in ENSO variability as evidenced by Figures 3cd. Interestingly, the largest changes for these quantities are observed over the Warm Pool region similarly to the study by Yeh et al. (2009) and are less sensitive to the concentration of greenhouse gases, suggesting a nonlinear response of the tropical Pacific.

Figure 3 also displays changes in α and β parameters induced by global climate change under different projection scenarios for the multi-model ensemble mean. The pattern of maps for the β parameter (Figures 3fh) denotes increase (decrease) in negative (positive) asymmetry associated with global warming in the Warm Pool (Cold Tongue) region. Interestingly, for the α parameter, a peculiar pattern of changes associated with increased GHG concentrations emerges (Figure 3eg): it consists of a region of decreased α-stability (decrease in deviation from Gaussianity i.e. $\Delta\alpha>0$) in the Cold Tongue region and a region of increased α-stability ($\Delta\alpha<0$) in the Warm Pool. In the far western equatorial Pacific the rising concentration of GHG tends to favour a more Gaussian-type behaviour ($\Delta\alpha>0$). The decrease in □over the Warm Pool region indicates a tendency towards more EEs in a warmer climate over this region. See Boucharel et al. (2011) for more explanations and details about the statistical confidence (and consistency among models) of Figure 3efgh.

This is consistent with the recent results by Yeh et al. (2009) who diagnosed an increase of the CP to EP El Niño ratio in a warmer climate. The increase in negative asymmetry over the Warm Pool region also suggests a tendency towards more and/or "stronger" cold events (relative to a warmer climate mean state) consistently with Timmermann (1999).

This raises the question of whether the tendency towards more El Niño events over the Warm Pool region (new "Modoki flavour" of El Niño) is directly related to the tropical Pacific mean state change associated with global warming (seen as an external forcing) or whether it is associated with changes in nonlinearity as an intermediate step in the process. In the next section, we will explore the relationships between the different types of El Niño and tropical Pacific nonlinearity, as measured by the parameter.

4. El Niño flavours and tropical Pacific nonlinearity.

In this section, we investigate the extent to which the change in El Niño type under global warming can be related to the change in nonlinearity. Whereas Yeh et al. (2009) suggest that the increase of CP El Niño frequency in a warmer climate may be associated with changes in mean state (mean thermocline depth and slope), we hypothesize here that it is also related to changes in nonlinearity of the tropical Pacific system. It is noteworthy that timescale interactions (low frequency mean state changes versus ENSO variability) through nonlinear processes are subject to decadal or inter-decadal modulation (see the review by An (2009)) so that diagnostics of global warming on such processes are not straightforward.

In particular, although observational records suggest a tendency towards more frequent CP El Niño in recent years, this may hide fluctuations in statistics on decadal to inter-decadal timescales. For instance, Kug et al. (2010) found a clear phase relationship between the frequency of occurrence of CP El Niño and low frequency changes in mean state in the Warm Pool region in the GFDL-CM2.1 model (see their Figure 13). It is therefore important to verify whether such low frequency variability can also be found in ENSO nonlinearity and the extent to which it can be influenced by global greenhouse warming.

The simple detection test proposed by Yeh at al. (2009) for distinguishing a CP El Niño from an EP El Niño is applied to data and model outputs. However, instead of using a fixed threshold of +0.5°C for the ENSO indices (Niño3 and Niño4 averaged over the boreal winter months of December-January-February) to account for El Niño, we used a threshold that depends on model variability (see Boucharel et al., 2011)

For sake of clarity, we chose to present results for one model among the most sensitive to global warming (seen as a change in tropical SST mean state), i.e. the MRI-CGCM2.3.2.A.

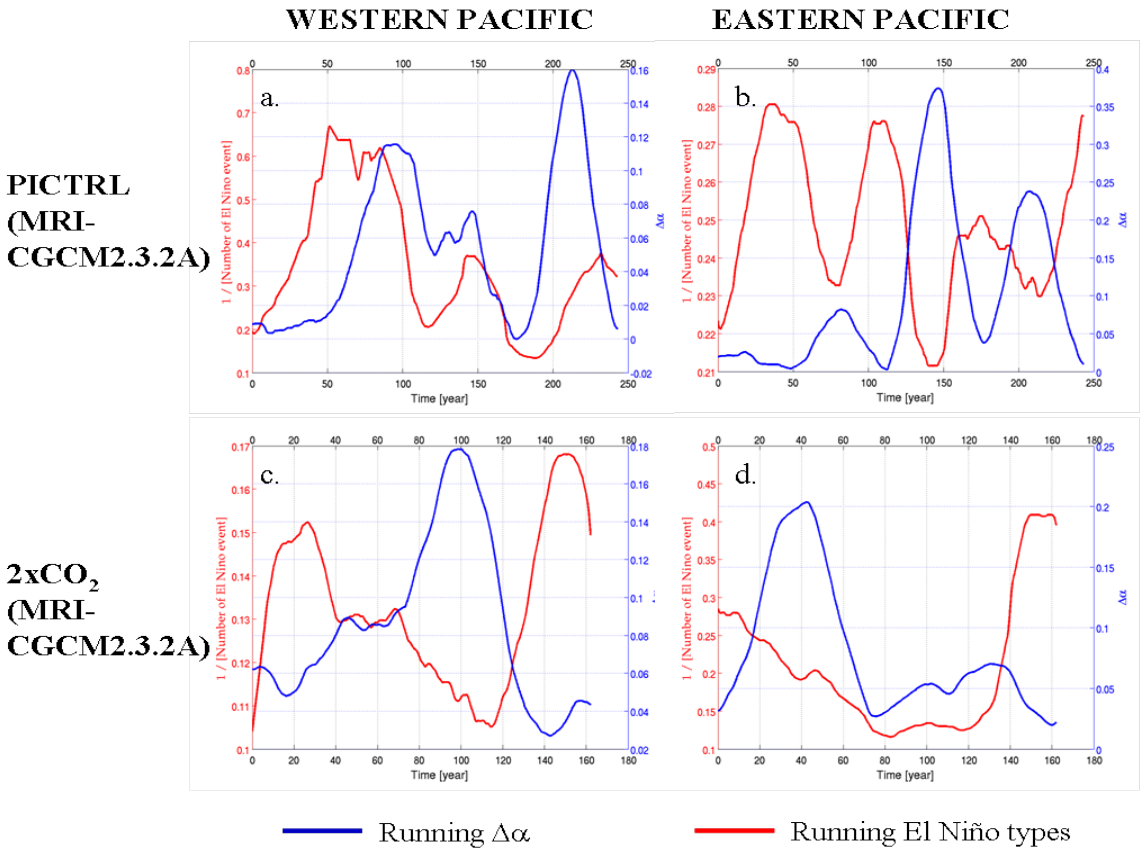

Figure 4. Running α parameter (27-year running windows) in blue lines (right panels for Niño3 and left panels for Niño4W) and running El Niño types frequency in red lines (left panels for Central Pacific and right panels for Eastern Pacific)

MRI-CGCM2.3.2.A PICTRL run (a. and b.)

MRI-CGCM2.3.2.A 2xCO2 run (c. and d.)

Figure 4 presents results for this model for the PICTRL and $2xCO_2$ scenarios. While the occurrence of so-called Modoki events does not seem to be related to nonlinear processes in a Pre-Industrial climate (correlation of -0.10, Figure 4a.), EP El Niño and over the Niño3 region exhibits a clear out of phase relationship (-0.66, Figure 4b.). Interestingly, the picture is reversed for this particular model under anthropogenic warming hypothesis. The correlation between El Niño Modoki and Niño4 index nonlinearity increases up to -0.80 (Figure 4c.), while the relationship between EP El Niño and $\Delta\alpha$ over the Niño3 region falls to 0.16 (Figure 4d.). This relationship between $\Delta\alpha$ and El Niño "flavours" appears to be a robust feature of the Tropical Pacific coupled system as it is clearly simulated by the majority of the selected models (Table 3 of Boucharel et al., 2011).

This raises the question of the evolution of low frequency tropical Pacific coupled modes under global warming hypothesis. Actually, beyond the inter-decadal alternation of favourable EP and CP El Niño periods (e.g. see the out of phase relationships between the red curves in the upper panels of Figure 4), Yeh et al. (2009) and Boucharel et al. (2011) diagnosed a dominance of the "Modoki/CP" mode in a warmer climate. The present study highlights the possible significant role of nonlinear mechanisms in driving this low frequency modulation of El Niño flavours.

5. Summary and Discussion

In the present study, we examined the response of ENSO statistics, particularly the high-order statistical moments through an alternative statistical framework, to abrupt changes in the mean climate background. Reconstructed data for the 20th century exhibited a clear modulation of ENSO nonlinearity (deviation of its statistics from a Gaussian distribution) according to the mean state. In particular, warm (cool) periods tend to favour more (less) nonlinear processes. This sensitivity to changes in mean state was further investigated in the CMIP3 database, using different scenario experiments provided by IPCC-AR4 to characterize different mean state. We found drastic changes in ENSO nonlinearity patterns in a warmer climate. The activity of nonlinear mechanisms tends to be translated from the Cold Tongue region to the central equatorial Pacific under greenhouse climate hypothesis.

This is consistent with recent studies which indicate that global warming may have a significant impact on El Niño characteristics, leading in particular to an increased occurrence of the so-called Modoki El Niño located in the central Pacific (Yeh et al., 2009). There are many processes that may be responsible for such changes. They involve complex interactions between mean state, ENSO variability and nonlinearity.

We evidenced here a low frequency modulation of the different El Niño flavours, namely the EP and CP El Niño, both in a Pre-Industrial and in a warmer climate. We found that the EP flavour was directly related to the Eastern Pacific nonlinearity in the PICTRL experiments, whereas the CP flavour does not seem to be driven by the central/western pacific nonlinear mechanisms. Interestingly, the picture is reversed in a warmer climate. These findings provide further arguments to the existence of a tropical Pacific natural coupled mode oscillating on decadal to inter-decadal timescales.

Further study is required to diagnose which of the numerous nonlinear processes is more influential in this low frequency modulation.

5. Bibliography

An, S.-I., and B. Wang, 2000: Interdecadal change of the structure of the ENSO mode and its impact on the ENSO frequency. J. Climate, 13, 2044-2055.

An, S.-I., and F.-F. Jin, 2001: Collective role of thermocline and zonal advective feedbacks in the ENSO mode. J. Climate, 14, 3421-3432.

An, S.-I., 2004: Interdecadal changes in the El Niño-La Niña asymmetry. Geophys. Res. Lett., 31:L23210, doi:101029/2004GL021299.

An, S.-I., and F.-F. Jin, 2004: Nonlinearity and asymmetry of ENSO. J. Climate, 17, 2399-2412.

An, S.-I., 2009: A review of interdecadal changes in the nonlinearity of the El Nino-Southern Oscillation. Theor. Appl. Climatol., 97, 29-40.

Ashok, K., S.K. Behera, S.A. Rao, H. Weng, and T. Yamagata, 2007: El Niño Modoki and its possible teleconnection. J. Geophys. Res., 112, C11007.

Belmadani, A., B. Dewitte, and S.-I. An, 2010: ENSO feedbacks and associated time scales of variability in a multi-model ensemble. J. Climate, accepted.

Boucharel, J., B. Dewitte, B. Garel, and Y. du Penhoat, 2009: ENSO's non-stationary and non-Gaussian character: The role of climate shifts. Nonlin. Proc. Geophys., 16, 453-473.

Boucharel, J., B. Dewitte, Y. du Penhoat, B. Garel, S.-W. Yeh, an J.-S Kug 2009: ENSO nonlinearity in a warming climate. In revision in Clim. Dynam.

Choi J., S.-I. An, B. Dewitte, and W.W. Hsieh, 2009: Interactive feedback between the tropical Pacific decadal oscillation and ENSO in a coupled general circulation model. J. Climate, 22, 6597-6611.

Dewitte, B., C. Cibot, C. Périgaud, S.-I. An, and L. Terray, 2007: Interaction between near-annual and ENSO modes in a CGCM simulation: Role of the equatorial background mean state. J. Climate, 20, 1035-1052.

DiNezio, P.N., A.C. Clement, G.A. Vecchi, B.J. Soden, B.P. Kirtman, and S-K. Lee, 2009: Climate response of the equatorial Pacific to global warming. J. Climate, 22, 4873-4892.

Guilderson, T.P., and Schrag D.P., 1998: Abrupt shift in subsurface temperatures in the tropical pacific associated with changes in El Niño. Science, 281, 5374, 240-243.

Guilyardi, E., A. Wittenberg, A. Fedorov, M. Collins, C. Wang, A. Capotondi, G.J. van Oldenborgh, and T. Stockdale, 2009: Understanding El Niño in Ocean–Atmosphere General Circulation Models: Progress and Challenges. Bull. Amer. Meteor. Soc., 90, 325-340.

Kaplan, A., M. Cane, Y. Kushnir, A. Clement, M. Blumenthal, and B. Rajagopalan, 1998: Analyses of global sea surface temperature 1856-1991. J. Geophys. Res., 103, 18,567-18,589.

Koutrouvelis, I.A., 1980: Regression-Type Estimation of the parameters of stable laws. J. Amer. Statist. Assoc., 75, N 372.

Kug, J.-S., J. Choi, S.-I. An, F.-F. Jin, and A.T. Wittenberg, 2010: Warm Pool and Cold Tongue El Nino events as simulated by the GFDL 2.1 coupled GCM. J. Climate 23, 1226-1239

Moon, B.-K., S.-W. Yeh, B. Dewitte, J.-G. Jhun, I.-S. Kang and B.P. Kirtman, 2004: Vertical structure variability in the equatorial Pacific before and after the Pacific climate shift of the 1970s. Geophys. Res. Lett. 31:L03203, doi: 10.1029/2003GL018829.

Rodgers, K.B., P. Friederichs, and M. Latif, 2004: Tropical Pacific Decadal Variability and Its Relation to Decadal Modulations of ENSO. J. Climate., 17, 3761-3774.

Schopf, P.S., and R.J. Burgman, 2006: A Simple Mechanism for ENSO Residuals and Asymmetry. J. Climate, 19, 3167–3179.

Timmermann, A., 1999: Detecting the nonstationary response of ENSO to greenhouse Warming. J. Atmos. Sci., 56, 2313-2325.

Timmermann, A., F.-F. Jin, and J. Abshagen, 2003: A nonlinear theory of El Niño bursting. J. Atmos. Sci., 60, 152-165.

Yeh, S.-W., J.-S. Kug, B. Dewitte, M.-H. Kwon, B.P. Kirtman, and F.-F. Jin, 2009: El Niño in a changing climate. Nature, 461, 511-514.

Zebiak, S.E., and M.A. Cane, 1987: A model of El Niño Southern Oscillation. Mon. Wea. Rev., 115, 2262,-2278

Observed freshening and warming of the western Pacific Warm Pool

Sophie Cravatte, Thierry Delcroix, Dongxiao Zhang, Michael McPhaden and Julie Leloup

Published in Climate Dynamics, 2009

Cravatte,S., T. Delcroix, D. Zhang, M. McPhaden and J. Leloup (2009), Observed Freshening of the warming Western Tropical Pacific and extension of the Warm/Fresh Pool in recent decades, Clim Dyn, doi 10.1007/s00382-009-0526-7.

The Warm Pool (WP) of the western tropical Pacific Ocean is characterized by some of the warmest seawaters of the global ocean, with Sea Surface Temperatures (SST) warmer than 28–29°C. Reaching depths of 100 m, the WP covers a large surface area of about 159106 km2 and contains an important warm water volume. Its warm waters supply the atmosphere with water vapor and heat, releasing latent heat and leading to convection and heavy rainfall in excess of 2–3 m per year. This high precipitation rate, associated with light winds in the region, induces Sea Surface Salinity (SSS) lower than 35 pss, and results in the formation of a relatively low density and stable oceanic mixed layer.

At the equator, the Warm and low-salinity waters of the WP are separated from the cold and saltier waters of the central Pacific by a sharp salinity front. The position of the eastern edge of the Warm Pool in the equatorial band, associated with an oceanic convergence zone and a salinity front, is a key parameter for ENSO dynamics and ocean–atmosphere interactions.

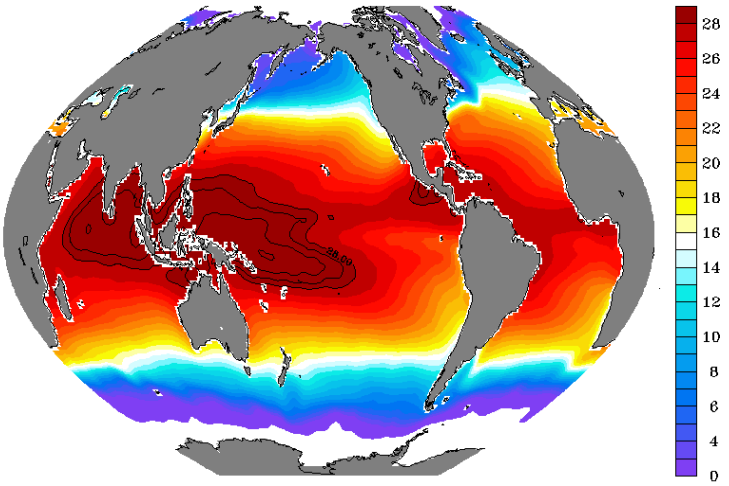

Figure 1: Mean SST from WOA2000

In a paper published in Climate Dynamics in 2009, S. Cravatte, T. Delcroix from IRD-LEGOS and coauthors from NOAA/PMEL and RSMAS used sea surface temperature and in situ sea surface salinity (SSS) data to address the central questions of whether Warm/Fresh Pool size, eastern extent and properties have changed in recent decades. Their results are striking: a significant surface freshening (up to 0.75 pss per 50 years) concurrent with an important surface warming (up to 1.2°C per 50 years, but typically from 0.2°C to 1°C per 50 years) was detected in the western tropical Pacific since 1955. Both warming and freshening are highly significant, since they reach at some locations five interannual standard deviations of the signal per 50 years. An increase in SSS is, in contrast, observed in regions of high evaporation, in the western Coral Sea and in the subtropical regions. Both geographical and seasonal SSS patterns are enhanced.

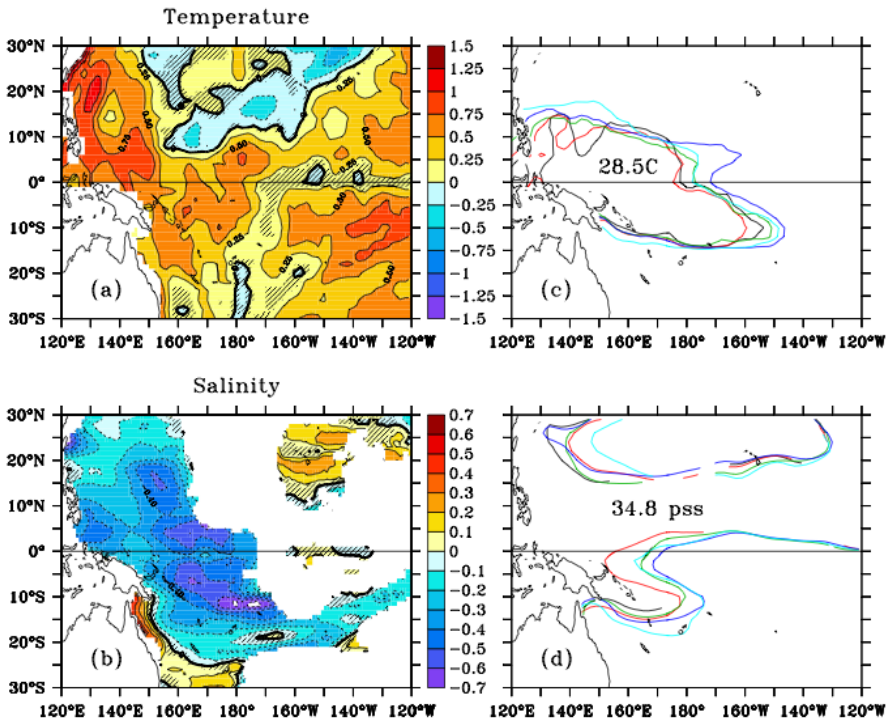

Figure 2 (@Climate Dynamics): Linear trends in SST (a) and SSS (b). Units are °C/50 years and pss/50 years. Positions of the 28.5°C isotherms (c) and of the 34.8 isohalines (d), averaged during 1956–1965 (black), 1966–1975 (red), 1976–1985 (green), 1986–1995 (blue) and 1996–2003 (light blue). The regions where the linear trends are not significant at the 90% confidence level are hatched in black

In response to these warming and freshening trends, the Warm/Fresh Pool extended both latitudinally and longitudinally at the surface during the past few decades. Interestingly, the warmest and freshest waters expanded the most in relative terms. The eastern edge of the Warm/Fresh Pool migrated eastward along the equator, as indicated by displacements of isohalines and isotherms. Strong decadal variability of the same magnitude as the long-term trend leads to a stronger eastward displacement from 1955 to the mid-1990s, and to a rather negligible displacement from 1978 to 2003. In the Southwestern tropical Pacific, the salinity front located under the South Pacific Convergence Zone also migrated southward and eastward. At decadal timescales, its longitudinal movements are opposite to those of the equatorial front, as they are at interannual timescales. Long-term trends are in the same direction though, which emphasizes that they are not simply the result of decadal variability or increased interannual variability.

Forcing fields that could be used to tentatively explain the observed freshening are not reliable. Alternatively, the " wet get wetter and dry get drier" paradigm associated with quasi-uniform tropical SST warming can provide useful guidance for the interpretation of the long-term SSS trends. Increased heating will enhance evaporation, while increased air moisture due to increase in saturation vapour pressure with temperature will produce more intense precipitation. They use a very simple model to predict the SSS changes using Clausius–Clapeyron scaling. Their results suggest that the increase of the mean hydrological cycle predicted by a simple Clausius–Clapeyron scaling is already happening, consistent with other recent works.

Following many previous studies, the paper suggests that salinity is an important indicator of climate change in the tropics. However, in some regions, decadal variability appears greater or on the same order of magnitude than longer term trends.

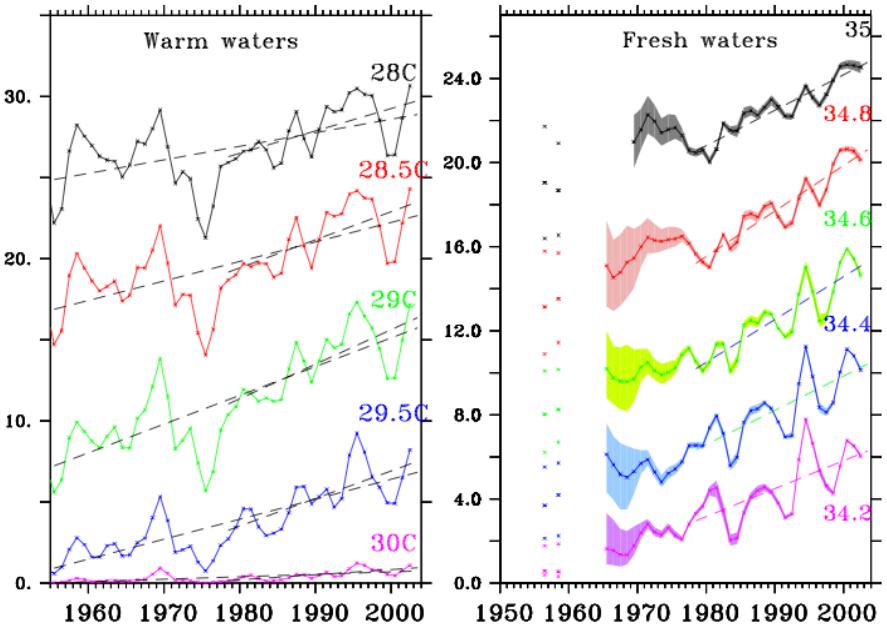

Figure 3 (@Climate Dynamics): Left: Time series of the surface area covered by waters warmer than SST thresholds. Right: Time series of surface area covered by waters fresher than SSS thresholds.

Low-frequency variations of the large-scale ocean circulation and heat transport in the North Atlantic from 1955–2008 in situ temperature and salinity data

T. Huck, A. Colin de Verdière, P. Estrade, F. Gaillard, R. Schopp, P. Bellec, R. Dussin

Laboratoire de Physique des Océans (UMR 6523 CNRS IFREMER IRD UBO), Brest, France

Abstract

On interdecadal timescales, the Atlantic meridional overturning circulation (AMOC) is thought to be in phase with the North Atlantic Sea Surface Temperatures (as measured by the Atlantic Multidecadal Oscillation – AMO – index). However, it appears that we have entered a positive phase of the AMO since 1995-2000 although we fear the Atlantic meridional overturning may be on a declining trend, as suggested by several observational and modelling studies. Here we constrain ocean models with temperature and salinity fields built on observations, and compare the results with various simple methods (namely diagnostic, robust diagnostic and prognostic), models (North Atlantic and global configurations at various resolutions), and forcings. Mean transports of heat and mass are sensitive to the method and model configuration, but their decadal variability is much more coherent and does not depend explicitly on the variations of the surface forcing, its influence being imprinted in the thermohaline structure. Multidecadal variations are of the order of 20% (0.15 PW in heat transport and 4 Sv in overturning), with large transports in the subpolar gyre in the early 1960's and mid 1990's, and low values in the mid 1970's. Declining transports of heat and mass are coherent in several models and methods since 1995, especially in the subpolar gyre, and opposite to the long term tendency from 1958 to 2008.

1. Introduction

Variations in the oceanic thermohaline structure have been documented over the last decades: surface intensified warming and changes in salinity, as well as deep water properties and formation rates [Dickson et al. 1996, 2002]. However the associated changes in the large-scale ocean circulation are poorly known, and deserve much interest in the context of the ongoing global warming and possible decay of the thermohaline circulation [Bryden et al. 2005; Gregory et al. 2005], or recent decline observed in the North Atlantic subpolar gyre [Häkkinen and Rhines 2004]. Several ocean models have been forced by atmospheric reanalysis forcings, but these forcings have significant uncertainties and well-known heterogeneities over the last 50 years. The main model deficiencies lie in formulation of subgrid-scale mixing with consequences on deep-water formation, usually impacting the overturning circulation on the long term. In situ data assimilation in such models on long time scales requires complex tools and delicate choices on the method, that largely influence the results. On the other hand, to avoid the need for accurate surface fluxes of heat and freshwater, one can use the observed temperature and salinity (TS) fields. Density providing the baroclinic velocities through the thermal wind relation, the barotropic part is obtained from the vorticity equation forced by the wind and a bottom pressure torque [Sarkisyan and Keonjiyan 1975]. Mellor et al. [1982] integrated this equation along f /H contours, whereas Holland and Hirschman [1972] used the dynamical part of numerical ocean models, although some adjustment of the bottom density field may be necessary [Ezer and Mellor 1994]. These methods have been applied to compare the pentads 1955–59 and 1970–74 [Greatbatch et al. 1991; Ezer et al. 1995], and more recently for 7 pentads from 1950 to 1994 using a finite element formulation [Myers et al. 2005]. NODC has made available global fields of TS pentadal anomalies from 1955–59 to 1994–98 based on hydrographic data. We will diagnose mean ocean currents from these fields to investigate the low-frequency variations of mass and heat transports in the North Atlantic. We first use three simple, well-documented methods: constant tracers, robust diagnostic, and short prognostic. Although the methods provide different results on the mean state, the low-frequency variations are rather coherent. Then, we implement only the robust diagnostic method in a global model continuous simulation with the seasonal cycle and TS anomaly fields updated to 2008.

2. First methodological step in a North Atlantic configuration with ROMS

The Regional Ocean Modeling System ROMS [Shchepetkin and McWilliams 2005] is used here, based on topography-following sigma coordinates. A smoothed bottom topography is required for accurate calculations of pressure gradients [Barnier et al. 1998 DSR]. We used a 1/2° resolution and 50 sigma levels to reproduce correctly the ocean bottom topography and capture the signature of the boundary currents in the TS climatologies. The model configuration spans from 10°N to 66°N in the Atlantic. The model is used to produce mean fields of T, S and velocities for each 5-yr period from 1955–59 to 1994–98. The initial TS fields were optimally interpolated on the model grid from the pentadal fields available on a 1°x1° grid and 33 z-levels. These pentadal fields were constructed from objectively analyzed anomalies of T and S down to 3000 m [Levitus et al. 2005; Boyer et al. 2005] and from the associated mean climatology (down to the bottom). Wind stress and surface fluxes are provided by the atmospheric reanalyses from NCEP [Kalnay et al. 1996

BAMS] and ECMWF ERA-40 [Uppala et al. 2005 QJRMS], averaged over the corresponding 5-yr periods. Three semi-diagnostic methods are implemented. Constant Tracers (hereafter CT): T and S are kept constant during the model integration, only the momentum equations are integrated in time and reach a steady state within months [Holland and Hirschman 1972]; the final velocity fields are averaged over months 6 to 12. Robust Diagnostic (RD): the tracer equations are now integrated in time with an additional relaxation to initial values with a timescale of 30 days [Sarmiento and Bryan 1982]; kinetic and potential energy adjusts within 6 months, and the final fields are averaged over the second year of integration. Short Prognostic (PR): the full dynamics and tracer equations are integrated for 45 days such that the barotropic velocities adjusts but the tracers do not drift away from the initial state [Ezer and Mellor 1994]; the final fields are averaged over the days 31 to 45. Rms differences between the initial and final TS fields are similar for both RD and PR methods (around 0.3 K at 100 m, 0.05 K at 1000 m and less than 0.01 K below 2000 m), although the former is in steady-state while the latter drifts rapidly from the initial state and longer prognostic integration would lead to much larger differences. Because the use of annual mean fields instead of seasonal cycle may be arguable, we have tested that the diagnostic transports of mass and heat on the annual mean climatology very closely resemble the mean of these diagnostics for the seasonal climatologies. Results are shown in Fig.1 for 1957-1996.

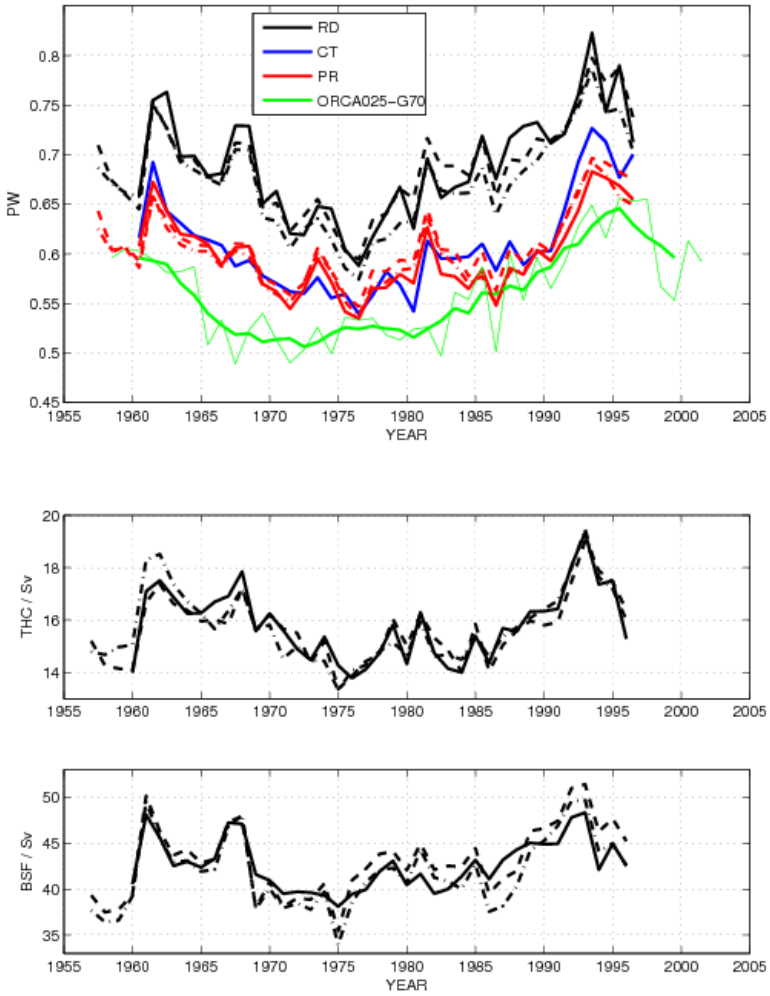

Figure 1: (top) Poleward heat transport maximum in the subpolar gyre (45-60°N) for the 3 diagnostic methods (RD robust diagnostic, CT constant tracers, SP short prognostic) implemented in a North Atlantic ROMS configuration using NODC pentadal TS anomalies and various forcings: ERA-40 (solid) or NCEP (dashed) 5-yr averaged surface fluxes, ERA-40 40-yr-averaged fields (dash-dotted); global prognostic reference simulation of the Drakkar project, ORCA025-G70, annual and pentadal means (green). (middle) Thermohaline circulation and (bottom) barotropic subpolar gyre intensity at 48°N, here for the RD method, show coherent variations with the poleward heat transport. Source: Huck et al. (2008).

3. Implementation of the robust diagnostic method in a global model configuration

Several limitations of the previous methods are addressed in this next step. First, to avoid open boundaries, a global model configuration is used with a ½° resolution, refined towards the equator: OPA ORCA05 [Molines et al. 2006]. The model integration is now continuous in time from 1958 to 2008. The surface forcing set is DFS4 [Brodeau et al. 2010] based on ERA-40 atmospheric reanalysis. The robust diagnostic method is implemented with relaxation time scale of 50 days in the upper 800m and 1 year in the deep ocean [Madec and Imbard 1996], although comparison with a uniform restoring field of 120 day shows no major change. The restoring TS fields, now varying in time and according to the seasonal cycle, are reconstructed from the annual or pentadal anomaly added to the monthly mean climatology. NODC pentadal fields are used for the period 1958 to 1996 as in the previous section. From 1997 to 2008, annual anomaly fields are used down to 2000m [von Schuckmann et al. 2009, Gaillard et al. 2009]. A twin prognostic experiment (ie. with no restoring in the ocean interior) is run for the same period. The restoring term efficiently removes incorrect trends in heat and salt content (not shown), and the evolutions of MOC and MHT diverge within 15 yr but show similar decadal variability (Fig. 2). Comparison is also performed with the Drakkar project reference experiment at ¼° resolution, ORCA025-G70 [Barnier et al. 2006]. In general, although the mean values of heat and mass transport

significantly vary from one model to the other, especially at 24°N, the decadal and longer variations show more coherence.

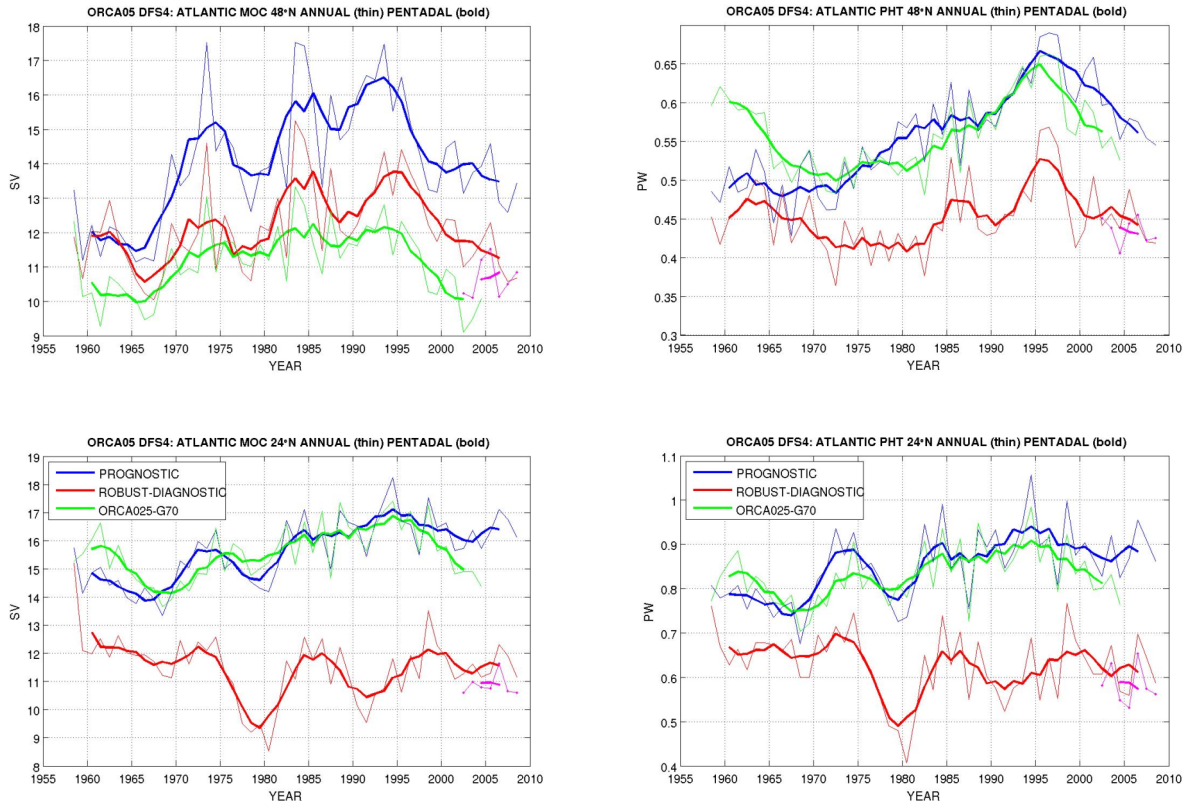

Figure 2: Synthesis of global ORCA05 simulations, prognostic (blue) and robust diagnostic (red), and comparison with Drakkar reference simulation (ORCA025-G70, green) for the evolution of the maximum meridional overturning circulation (MOC) and meridional heat transport (PHT) at 24°N (bottom) and 48°N (top) in the Atlantic. Thin (bold) lines are annual (pentadal) means. Dots correspond to average over the last 2 years for "equilibrium" 12-yr long simulations with restoring and DFS4 forcing of the year repeated (magenta). The decline of mass and heat transport at 48°N since 1995, opposite to the long term 1958-2008 tendency, appears as the most robust signal.

4. Discussion and conclusion

This work provides an estimate of the low-frequency variability in the North Atlantic circulation based on in situ TS data using simple methods: diagnostic, robust-diagnostic and short prognostic. Without finely tuning the model configuration or parameterizations, the variability in mass and heat transports associated with the thermohaline changes has been successfully captured in the subpolar gyre, as compared to state-of-the-art prognostic models: energetic barotropic and overturning circulations drive high heat transport in the early 60's and mid 90's, whereas both circulations and heat transport are at the lowest in the mid 70's, and declining since 1995, in agreement with observational estimates attributed to NAO forcing [Curry and McCartney, 2001]. Our methods also point out an apparent phase opposition in heat transport between the subtropical and subpolar gyres, that could result from the delayed adjustment of the meridional overturning at lower latitude to the low-frequency NAO forcing [Eden and Jung 2001]. The original idea of relying on in situ observations rather than changes in the surface forcing to investigate the variations of the ocean circulation provides an alternative to prognostic hindcast models, with or without assimilation, that avoids potential model drift associated with uncertainties in both subgrid-scale processes parameterizations and surface fluxes. Yet let us recall that these are dynamical and not thermodynamical methods: they allow only limited insight in heat or salt budgets for instance. The pentadal/annual TS fields are certainly not perfectly constrained over the last decades, especially at depth, and due to the scarcity of salinity data: the robustness of our results should be investigated with the use of alternative products, analyzed on isopycnal surfaces for instance. The large smoothing in the NODC data set, as discussed by Myers et al. [2005], may also have some influence on our results, as well as the transition from NODC to LPO fields. A radical change occurred in the observing system since 2003 with Argo, that allows to build reliable annual fields of TS for the upper 2000m, and we have shown this is sufficient to reconstruct most of the large-scale circulation changes. See Huck et al. [2008] for a detailed analysis of the results.

References

Barnier, B., et al., 2006: Impact of partial steps and momentum advection schemes in a global ocean circulation model at eddy permitting resolution. Ocean Dyn., 56, 1616-7341.

Boyer, T. P., et al., 2005: Linear trends in salinity for the world ocean, 1955–1998, Geophys. Res. Lett., 32, L01604.

Brodeau, L., et al., 2010: An ERA40-based atmospheric forcing for global ocean circulation model. Ocean Model., 31, 3-4, 88-104.

Bryden, H. L., H. R. Longworth, S. A. Cunningham, 2005: Has the Atlantic overturning circulation slowed?, Nature, 438, 655 – 657.
Curry, R. G., M. S. McCartney, 2001: Ocean gyre circulation changes associated with the NAO, J. Phys. Oceanogr., 31, 3374– 3400.

Dickson, B., et al., 2002: Rapid freshening of the deep North Atlantic Ocean over the past four decades, Nature, 416, 832– 837.

Dickson, R., et al., 1996: Long-term coordinated changes in convective activity of the North Atlantic, Prog. Oceanogr., 38, 241– 295.

Eden, C., T. Jung, 2001: North Atlantic interdecadal variability: Oceanic response to the NAO (1865-1997). J. Clim., 14, 676– 691.

Ezer, T., G. L. Mellor, 1994: Diagnostic and prognostic calculations of the North Atlantic circulation and sea level using a sigma coordinate ocean model, J. Geophys. Res., 99, 14,159–14,172.

Ezer, T., et al., 1995: On the interpentadal variability of the North Atlantic Ocean. J. Geophys. Res., 100, 10,559 – 10,566.

Gaillard, F., et al., 2009: Quality control of large Argo datasets. J. Atmos. Ocean. Technol., 26 (2),. 337-351.

Greatbatch, R. J., J. Xu, 1993: On the transport of volume and heat through sections across the North Atlantic: Climatology and the pentads 1955 – 1959, 1970 – 1974, J. Geophys. Res., 98, 10,125 – 10,142.

Gregory, J. M., et al., 2005: A model intercomparison of changes in the Atlantic thermohaline circulation in response to increasing atmospheric CO2 concentration, Geophys. Res. Lett., 32, L12703, doi:10.1029/2005GL023209.

Häkkinen, S., P. B. Rhines, 2004: Decline of subpolar North Atlantic circulation during the 1990s, Science, 304, 555 – 559.

Holland, W. R., A. D. Hirschman, 1972: A numerical calculation of the circulation in the North Atlantic Ocean, J. Phys. Oceanogr., 2, 336 – 354.

Huck, T., et al., 2008: Low-frequency variations of the large-scale ocean circulation and heat transport in the North Atlantic from 1955-1998 in-situ temperature and salinity data. Geophys. Res. Let., 35, L23613.

Levitus, S., J. Antonov, T. Boyer, 2005: Warming of the world ocean, 1955 – 2003, Geophys. Res. Lett., 32, L02604.

Madec, G., M. Imbard, 1996: A global ocean mesh to overcome the North Pole singularity. Clim. Dyn., 12, 381-388.

Mellor, G. L., et al., 1982: A diagnostic calculation of the general circulation of the Atlantic Ocean, Deep Sea Res. A, 29, 1171-1192.

Molines, B. et al., 2006: Definition of the global 1/2° experiment with CORE forcing, ORCA05-G50. LEGI report DRA-1-11-2006.

Myers, P. G., S. Grey, K. Haines, 2005: A diagnostic study of interpentadal variability in the North Atlantic Ocean using a finite element model, Ocean Modell., 10, 69–81.

Sarkisyan, A. S., V. P. Keonjiyan, 1975: Review of numerical ocean circulation models using the observed density field, Numerical Models of Ocean Circulation, pp. 76– 93, Natl. Acad. of Sci., Washington, D. C.

Sarmiento, J. L., K. Bryan, 1982: An ocean transport model for the North Atlantic, J. Geophys. Res., 106, 16,711 – 16,728.

Shchepetkin, A., J. C. McWilliams, 2005: The Regional Oceanic Modeling System: A split-explicit, free-surface, topography-following coordinate ocean model, Ocean Modell., 9, 347– 404.

von Schuckmann, K., F. Gaillard, P.-Y. Le Traon, 2009: Global hydrographic variability patterns during 2003-2008. J. Geophys. Res., 114, C9, C09007, doi:10.1029/2008JC005237.

Ocean wave research in France, 2007-2010

Fabrice Ardhuin, Ifremer, Brest, France

Recent developments in the investigations of ocean waves are marked by their connections with other geophysical disciplines, from air-sea interactions and remote sensing to seismology, through coastal oceanography. Indeed the current wave of progress toward ever more realistic numerical models of sea states (e.g. WISE group 2007) has been based on the analysis of a wider range of observations from various types of instruments. Among these, the space-borne synthetic aperture radar data acquired in "wave mode" by the Advanced SAR on board ESA's Envisat mission, a legacy of the ERS 1 and 2 missions thanks to Klaus Hasselmann, has been used to measure the dissipation rates of trans-oceanic swells, with unprecedented accuracy (Ardhuin et al. 2009). The e-folding scales of swells was found to vary systematically with wave steepness and period, from 2000 to over 20000 km for wave periods in the range 13 to 18s. This measurement gave us the biggest missing piece in the energy balance of wave fields at global scale. A tentative theory has been proposed for the observed nonlinear dissipation rate, with stronger dissipation for steeper swells, which may reconcile observations of wave-driven winds and the persistence of swells at global scales. Yet a full understanding of the air-sea boundary layer is still missing.

Based on this observation, the parameterizations of wave dissipation processes have been re-established, with more accurate numerical wave models (Ardhuin et al. 2010). This accuracy was verified against measurements of wave heights, directional wave parameters spectral distributions which include some parameters relevant for many geophysical applications. In particular the mean square slopes of the sea surface can now be estimated with a relative accuracy of about 15% r.m.s., which thus includes the long wave contribution to the slopes. This opens new perspectives for the processing of remote sensing data, in particular for the sea surface salinity retrievals from the SMOS and Aquarius missions, for which the slopes induced by the long waves can produce deviations in the measured quantities (brightness temperatures) equivalent to a salinity change by up to 3 P.S.U. Likewise, these effort make it now possible to improve the sea state bias estimates for more accurate estimates of sea level using altimetry (Tran et al. 2010).

A more challenging area of application, because of the poor knowledge of the directional wave properties, is the estimation of seismic noise sources from ocean wave spectra. Ardhuin et al. (manuscript submitted to J. Geophys. Res.) have demonstrated the capability to reproduce observed seismic spectra with unprecedented accuracy, for most of the global seismic network stations (e.g. figure 1). Using the theory by Hasselmann (1963), this numerical model has revealed that seismic noise sources are strongest in the middle of ocean basins, although many land-based seismometers are mostly sensitive to coastal sources only. This determination of seismic source locations is an important step for better interpretations of seismic noise correlations (Shapiro and Campillo 2004). This seismic noise model was also used to refine estimates of sea states from seismic noise which should provide more accurate analyses of past wave climates, as already proposed by Bernard (1990) or Grevemeyer et al. (2000).

There has also been strong developments in the theoretical formulation of the interaction of waves, currents and turbulence (e.g. Ardhuin et al. 2008), which are now being implemented in three-dimensional primitive equation models for the investigation of nearshore flows with a wide variety of applications: from sediment dynamics to water quality or storm surges. In this area the parameterization of bottom friction and mixing will still require more work, while observations are still scarce and limited. The general improvement in our understanding of wave dynamics should not conceal the formidable questions that are still unaswered. These include the effect of breaking waves on fluxes across the ocean surface. This is probably the most important problem at hand, either for upper ocean mixing (e.g. Rascle and Ardhuin 2009) or for the production of marine aerosols which have a key role in the climate regulation by clouds. On this front we can mention the remarkable measurements by Reul et al. (2008) of modifications of the wind stress by breakers. These observations and others made internationally are feeding the development of the next generation of wave model parameterization, which should aim at predicting wave breaking statistics for many geophysical and other applications.

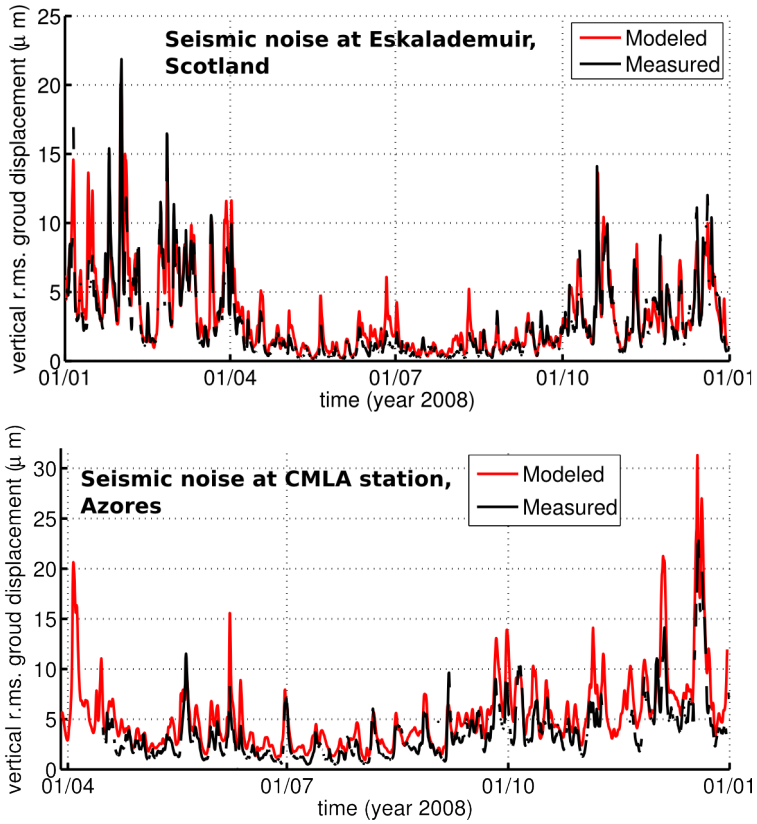

Figure 1: Observed and modelled ground motion caused by secondary microseisms in the North Atlantic, as recorded by two seismic stations. The model is described in Ardhuin et al. (submitted) using the latest improvements in numerical wave modelling. Earthquakes have been filtered out from the measured time series.

References

Ardhuin F., B. Chapron, and F. Collard, "Observation of swell dissipation across oceans," Geophys. Res. Lett., vol. 36, p. L06607, 2009a.

Ardhuin F., E. Rogers, A. Babanin, J.-F. Filipot, R. Magne, A. Roland, A. van der Westhuysen, P. Que□eulou, J.-M. Lefevre, L. Aouf, and F. Collard, "Semi-empirical dissipation source functions for wind-wave models: part I, definition, calibration and validation," J. Phys. Oceanogr., vol. 40, p. in press, 2010.

F. Ardhuin, E. Stutzmann, M. Schimmel, and A. Mangeney, "Revealing ocean wave sources of seismic noise," J. Geophys. Res., 2010. submitted.

F. Ardhuin, N. Rascle, and K. A. Belibassakis, "Explicit waveaveraged primitive equations using a generalized Lagrangian mean," Ocean Modelling, vol. 20, pp. 35–60, 2008.

P. Bernard, "Historical sketch of microseisms from past to future," Phys. Earth Planetary Interiors, vol. 63, pp. 145–150, 1990.

I. Grevemeyer, R. Herber, and H.-H. Essen, "Microseismological evidence for a changing wave climate in the northeast Atlantic Ocean," Nature, vol. 408, pp. 349–1129, 2000.

K. Hasselmann, "A statistical analysis of the generation of microseisms," Rev. of Geophys., vol. 1, no. 2, pp. 177–210, 1963.

Rascle N. and F. Ardhuin, "Drift and mixing under the ocean surface revisited. stratified conditions and model-data comparisons," J. Geophys. Res., vol. 114, p. C02016, 2009. doi:10.1029/2007JC004466.

N. Reul, H. Branger, and J.-P. Giovanangeli, "Air flow structure over short-gravity breaking water waves," Boundary-Layer Meteorol., vol. 126, pp. 477–705, 2008.

Shapiro, N. M. & Campillo, M. 2004 Emergence of broadband Rayleigh waves from correlations of the ambient seismic noise. Geophys. Res. Lett. 31, L07614. doi:10.1029/2004GL019491

Tran N., D. Vandemark, S. Labroue, H. Feng, B. Chapron, H. L. Tolman, J. Lambin, and N. Picot, “The sea state bias in altimeter sea level estimates determined by combining wave model and satellite data,” J. Geophys. Res., vol. 115, p. C03020, 2010.

WISE Group: «Wave modelling - the state of the art». Progress in Oceanography Vol. 75, pp. 603-674, 2007.

Coastal patterns tracking: a lagrangian approach

Philippe FRAUNIE

Several investigations have been recently conducted in coastal areas in the framework of collaborative field campaigns granted and organized by research agencies and national oceanography administrations (INSU, SHOM, IFREMER) together with university laboratories.

Process oriented measurements and modeling have been performed concerning wind induced and baroclinic small scale features including vortices, filaments, fronts, alongshore current stability, internal tides and waves for better prediction of retention structures and confinement barriers.

In addition to high resolution RV cruises, satellite and HF radar synoptic mapping of the sea surface and vertical profilers and moorings, lagrangian measurements from drifting buoys and gliders have been extensively analysed. Especially, complementary deployment strategy allowed to validate each other measurements and models for high frequency patterns and sudden events both in tidal (bay of Biscay) and microtidal (Gulf of Lions, Adriatic sea) coastal environments. Figures 1 to 3 give examples of investigations in different coastal areas.

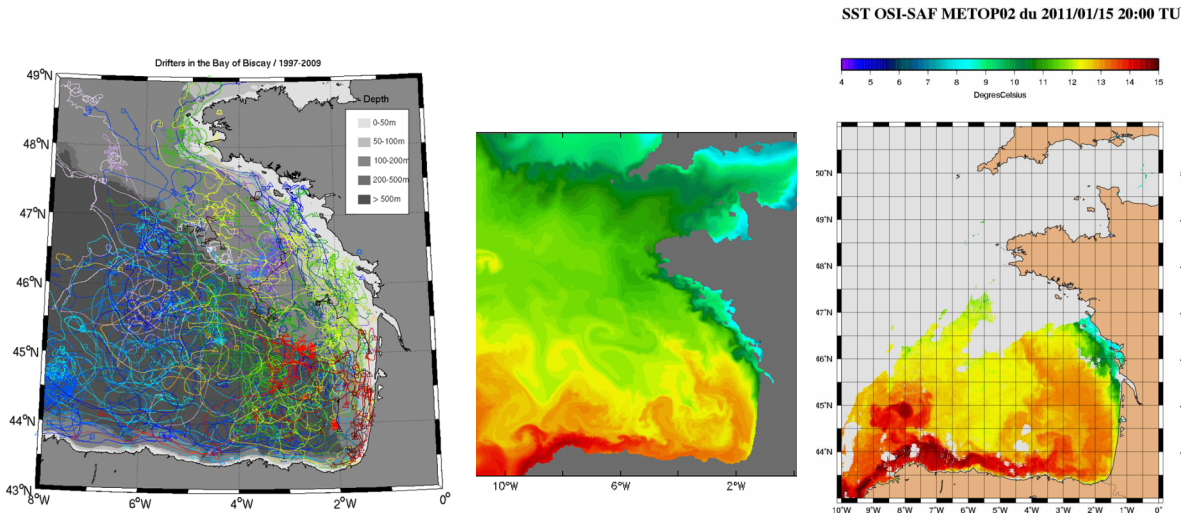

Fig 1. Drifted buoys trajectories in the bay of Biscay (EPIGRAM project, 2009-2012) (Charria et al) and Navidad event (southern warm waters inflow on the shelf) (Le Cann, Serpette et al)

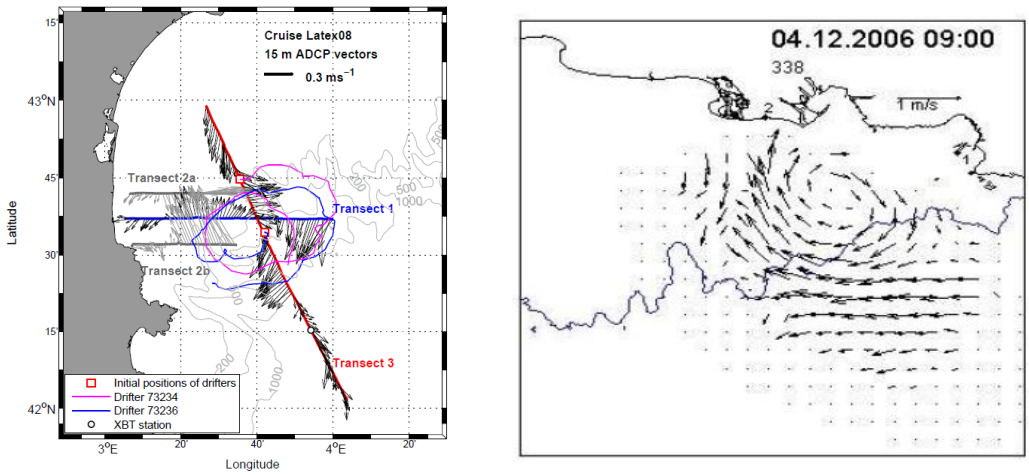

Fig 2. Anticyclonic vortices in the Gulf of Lions (LATEX and ECOLO experiments) ADCP, drifters and HF radar measurements) (Hu et al., 2010, Allou et al 2009)

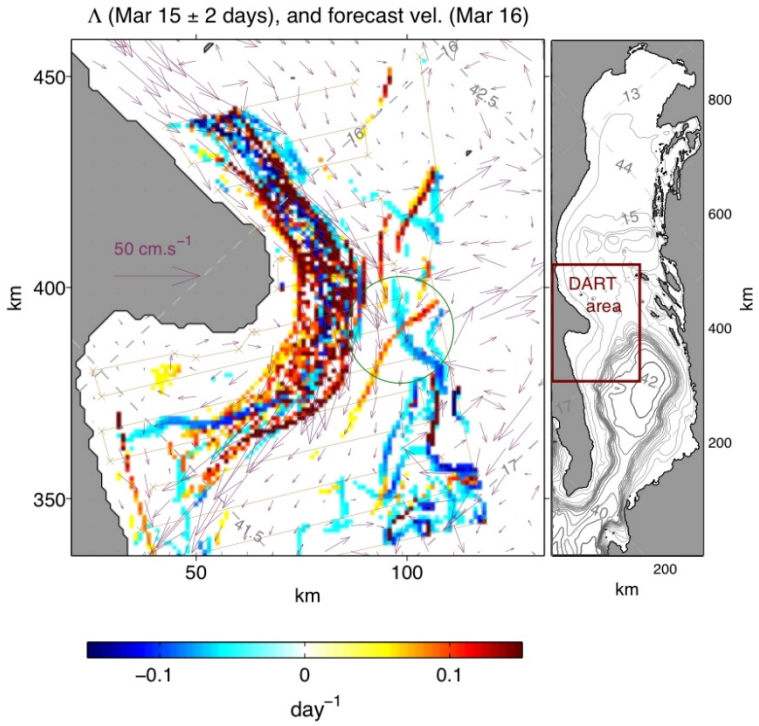

Fig. 3 Model-based directed drifter launches in the Adriatic Sea:
Results from the DART experiment, Haza et al., 2007.

New projects are concerning better understanding of coastal and internal waves from theoretical and high resolution long series measurements (Bouruet Aubertot et al, Zeitline et al).

Selected references :

Bay of Bisacy project :

Marsaleix P., Ulses C., Pairaud I., Herrmann M.J., Floor J.W., Estournel C., Auclair F., 2009. Open boundary conditions for internal gravity wave modelling using polarization relations. Ocean Modelling, 29, 27-42.

Le Hénaff M., De Mey P., Marsaleix P., 2009. Assessment of observational networks with the Representer Matrix Spectra method-application to a 3D coastal model of the Bay of Biscay. Ocean Dynamics, 59, 3-20

Philippe Grosso, Marc Le Menn, Jean-Louis De Bougrenet De La Tocnaye, Zong Van Wu, Damien Malarde, 2009. Deep-Sea Research 1 57 (2010) 151- 156. Practical versus absolute salinity measurements: New advances in high performance seawater salinity sensors.

G. Reverdin, J. Boutin, N. Martin, A. Lourenco, P. Bouruet-Aubertot, A. Lavin, J. Mader, P. Blouch, J. Rolland, F. Gaillard, P. Lazure, 2010. accepted JAOT-O. Temperature measurements from surface drifters.

Michel S., Vandermeirsch F. and Lorance, P., 2009. Aquat. Living Resour., volume 22, 447-461. DOI: 10.1051/alr/2009054. Evolution of upper layer temperature in the Bay of Biscay during the last 40 years.

Bonneton, P., Bruneau, N., Marche, F. and Castelle, B. 2010. DCDS-S, in press. Large-scale vorticity generation due to dissipating waves in the surf zone.

Cienfuegos, R., Barthelemy, E. and Bonneton, P. 2010. J. Waterway, Port Coastal and Ocean Engrg, 136, 10-26. A wave-breaking model for Boussinesq-type equations including mass-induced effects.

Bruneau, N., Castelle, B., Bonneton, P., Pedreros, R., Almar, R., Bonneton, N., Bretel, P., Parisot, J-P. and Sénéchal, N. 2009. Continental Shelf Res, 29,1650–1662, doi:10.1016/j.csr.2009.05.005. Field observations of an evolving rip current on a meso-macrotidal well-developed inner bar and rip morphology.

Lannes D., Bonneton P. 2009. Physics of Fluids 21 (1), 016601 (9 pages), DOI: 10.1063/1.3053183. Derivation of asymptotic two-dimensional time-dependent equations for surface water wave propagation.

Ardhuin, F., B. Chapron, and F. Collard, 2009. Geophysical Research Letters, vol. 36, p. L06607. Strong decay of steep swells observed across oceans.

Ardhuin, F., L. Marié, N. Rascle, P. Forget, and A. Roland, 2009. Journal of Physical Oceanography, 39, 2820—2838. Observation and estimation of Lagrangian, Stokes and Eulerian currents induced by wind and waves at the sea surface.

Collard, F., Ardhuin, F., B. Chapron, 2009. Journal of Geophysical Research, 114, C07023. Routine monitoring and analysis of ocean swell fields using a spaceborne SAR.

V. Rossi, C. Lopez, E. Hernandez-Garcia, J. Sudre, V. Garcon, and Y. Morel, 2009. Nonlin. Processes Geophys., 16, 557–568. Surface mixing and biological activity in the four Eastern Boundary Upwelling.

Cécile Renaudie, Rémy Baraille, Yves Morel, Gwenaëlle Hello, Hervé Giordani, 2009. Ocean Modelling, 30, 178-189. Adaptation of the vertical resolution in the mixed layer for HYCOM.

V. Rossi, Y. Morel and V. Garçon, 2009. Ocean Modelling, doi : 0.1016/j.ocemod.2009.10.002. Effect of the wind on the dynamics of the shelf : formation of a secondary upwelling along the continental margin.

B. Le Cann and A. Serpette, 2009. Continental Shelf Research, doi:10.1016/j.csr.2008.11.015. Intense warm and saline upper ocean inflow in the southern Bay of Biscay in autumn-winter 2006-2007.

Le Boyer A., Cambon G., Daniault N., Herbette S., Le Cann B., Marié L., Morin P, 2009. Cont. Shelf. Res. (29) 1026-1037. Observations of the Ushant tidal front in september 2007

L. Marié, 2009. Nonlin. Processes Geophys. (17), 49-63, 2010. A study of the phase instability of quasi-geostrophic Rossby waves on the infinite beta-plane to zonal flow perturbations.

Rascle, N., F. Ardhuin, 2009. Journal of Geophysical Research, 114, C02016, doi:10.1029/2007JC00446. Drift and mixing under the ocean surface. Part 2: Stratified conditions and model-data comparisons.

Y. Morel and L. Thomas, 2009. Ocean Modelling, doi:10.1016/j.ocemod.2009.01.002. Ekman drift and vortical structures.

Mediterranean sea projects :

Hu, Z.H., Petrenko, A.A., Doglioli, A.M., Dekeyser, I. (2011), Numerical Study of eddy generation in the western part of the Gulf of Lion, JGR, submitted

Hu, Z.H., Petrenko, A.A., Doglioli, A.M., Dekeyser, I. (2010), Study of coastal eddies : application in the Gulf of Lion. J. Marine Syst., accepted.

Hu, Z.H., Doglioli, A.M., Petrenko, A.A., Marsaleix, P., Dekeyser, I. (2009), Numerical simulations of eddies in the Gulf of Lion. Ocean Model., Vol. 28/4, pp. 203-208, doi : 10.1016/j.ocemod.2009.02.004

Allou A., Forget P. and J.L. Devenon (2009) Submesoscale vortex structures at the entrance of the Gulf of Lions in the Northwestern Mediterranean Sea. Cont. Shelf Res., 30: 724-732

André G., Garreau P., Fraunié P. (2009) Mesoscale slope current variability in the Gulf of lions. Interpretation of in-situ measurements using a 3D model, Cont. Shelf Res. 29: 407-423

Casella E., Molcard A., Provenzale A. , Simulations of sub-mesoscale eddies in the Ligurian Sea. J. Mar. Syst., to appear.

Dufois F., Garreau P., Le Hir P., Forget P. (2008), Wave and current-induced bottom shear stress distribution in the Gulf of Lions. Continental Shelf Res., 28(15), pp.1920-1934.

Forget P. and G. André (2007), Can satellite-derived chlorophyll imagery be used to trace surface dynamics in coastal zone ? A case study in the Northwestern Mediterranean Sea. Sensors 7 884-904.

Forget, P., M. Saillard, and P. Broche, (2006) Observations of the sea surface by coherent L band radar at low grazing angles in a nearshore environment, J. Geophys. Res., 111 C09015, doi:10.1029/2005JC002900.

Haza A., Ozgokmen T.M., Griffa A., Molcard A., Poulain P.-M., Peggion G. (2010), Transport properties in small scale coastal flows : relative dispersion from VHF radar measurements in the Gulf of La Spezia, Ocean Dynam.,sous presse.

Haza, A. C.,A. Griffa, P. Martin, A. Molcard, T. M. Ozgokmen, A. C. Poje, R. Barbanti, J. Book, P. M. Poulain, M. Rixen, P. Zanasca (2007), Model-based directed drifter launches in the Adriatic Sea: Results from the DART Experiment, Geophys. Res. Letters 34 L10605 , doi:10.1029/2007GL029634

Jouon A., Douillet P., Ouillon S., Fraunié P. (2006), Calculations of hydrodynamic time parameters in a semi-opened coastal zone using a 3D hydrodynamical model, Cont. Shelf Res., 26, 1395-1415.

Langlais C., Barnier B., Molines J.M., Fraunié P., Jacob D., Kotlarski S. (2009) Evaluation of dynamically downscalled atmospheric reanalysis in the prospect of forcing long term simulations of the ocean circulation in the Gulf of Lions.,Ocean Modelling 30: 270-286

Maps F, Plourde S, Zakardjian B (2010) Control of dormancy by lipid metabolism in Calanus finmarchicus: a population model test , Mar. Ecol. Progr. Ser. 403 165-180), doi:10.3354/meps08525

Molcard A., Poulain P.M., Forget P., Griffa A., Barbin Y., Gaggelli J., De Maistre J.C., Rixen M. (2009), Comparison between VHF radar observations and data from drifter clusters in the Gulf of La Spezia (Mediterranean Sea), J. Mar. Sys., 78:79-89./

Taillandier, V., A. Griffa, A. Molcard (2006) A variational approach for the reconstruction of regional scale Eulerian velocity fields from Lagrangian data, Ocean Modelling 13(1): 1-24

F. Bouchut and V. Zeitlin, A robust well-balanced scheme for multi-layer shallow water equations, 2010, Discr. and Cont. Dyn. Systems, 13, 739 – 758 .

F. Bouchut, E. Scherer, and V. Zeitlin, Nonlinear adjustment of a front over escarpment, 2008, Phys. Fluids, 20, 016602-1 – 016602-12.

Bouruet-Aubertot, P., van Haren, H., Lelong, M.P. 2010 "Stratified inertial subrange in the boundary layer of Rockall channel", J. Phys. Oceanogr., 40, 2401- 2417..

Bouruet-Aubertot, P., Mercier, H., Gaillard, F., Lherminier, P. 2005. Evidence of strong inertio-gravity waves during POMME experiment, J. Geophys. Res., 110, doi 10-1029/2004JC002747

Ferrarri, R., Wunsch, C. 2010. The distribution of eddy kinetic and potential energies in the global ocean. Tellus, 62A, 92-108.

J. Gula, R. Plougonven, and V. Zeitlin, Ageostrophic instabilities of fronts in a channel in a stratified rotating fluid, 2009, J. Fluid. Mech., 627, 485 - 507 .

J. Gula and V. Zeitlin, Instabilities of buoyancy-driven coastal currents and their nonlinear evolution in the two-layer rotating shallow water model. I. Passive lower layer, 2010, J. Fluid Mech. 659, 69 - 93.

J. Gula , V. Zeitlin and F. Bouchut, Instabilities of buoyancy-driven coastal currents and their nonlinear evolution in the two-layer rotating shallow water model. II. Active lower layer, 2010, J. Fluid Mech. – in press.

Komori, N., Ohfuchi, W., Taguchi, B., Sasaki H., Klein, P. 2008 « Deep ocean inertia-gravity waves simulated in a high-resolution global coupled atmosphere-ocean gcm » Geophys. Res. Lett., 35, 1897-1915.

Le Vaillant, X., Cuypers, Y., Bouruet-Aubertot, P., Vialard, J., McPhaden, M. 2010. «Generation and propagation of near-inertial baroclinic waves during Cirene experiment : energy fluxes and impact on vertical mixing", submitted to J. Geophys. Res.

Medvedev, S.B., Zeitlin, V. "Turbulence of near-inertial waves in the continuously stratified fluid" Phys. Letters A, v. 371, p.221-227

G. Reznik and V. Zeitlin, Resonant excitation of trapped waves by free inertia-gravity waves in coastal waveguide, and their nonlinear evolution, 2010 J. Fluid Mech. – accepted.

Scherer E. and V. Zeitlin, Stability and nonlinear evolution of coupled geostrophic density fronts, 2008, J. Fluid. Mech., 613, 309 - 327.

Winters, K., Bouruet-Aubertot, P., Gerkema, T. 2010. "Critical reflexion and abyssal trapping of near-inertial waves on a beta plane", submitted to J. Fluid Mech., in revision

Zervakis, V., Levine, M.D. 1995. Near-inertial energy propagation from the mixed layer: theoretical considerations. J. Phys. Oceanogr., 25, 2872-2889.